

# Modeling and Identification of Supply Chains on Subspace Basis

T. Vadvári<sup>1</sup>, P. Várlaki<sup>1</sup>

<sup>1</sup>Széchenyi István University, System Theory Laboratory  
Egyetem tér 1., 9026 Győr, Hungary  
E-mail: varlaki@sze.hu

**Abstract:** Logistical processes play crucial role in many systems where the resources as well as tasks related to them are to be organized or scheduled in order to increase the throughput of the system, thus the rate of servicing demands. In this paper let us focus on loading systems and supply chains which represent a specific type of logistical processes. In order to increase the throughput of a loading system, delays caused by its certain subsystems are to be minimized. In our previous studies we have already shown how loading systems can be identified on subspace basis and how the relation between its certain parameters can be characterized. In contrast this paper is aimed to show through examples how system delays affect the efficiency of subspace based identification applied on loading systems.

**Keywords:** *Subspace identification, queuing models, supply chains, modeling*

## 1. Introduction

Supply chains as a specific category in logistics might be represented as a network of nodes representing facilities that perform some actions related first of all to manufacturing, transportation and distribution of products. Depending on the participant of the supply chain such a network may consist of many interconnected nodes, with specific characteristics [1]. Thus, the behavior of a complex supply chain may depend on many factors. The topology of the network may change as well especially when a facility becomes unable to fulfill its function due to some reasons. The authors in [2] for example deal with so called integrated supply chain optimization problems where the locations of facilities, customer allocations, etc. are considered as well when facilities are subject to disruption risks.

In order to identify these factors as well as their impact on the whole chain, modeling and identification of the system has to be performed. As in many fields also in logistics modeling and identification approaches play significant role especially when accurate models of complex logistical processes (LP) have to be designed. Authors in [3] consider

queuing models to compute the response time for the delivery of items. Proper supply chain models may be helpful to predict various features related to the modeled system, such as the response time or in case of supply chains the delivery cycle time, customer order path (related to time spent in different channels), etc. In addition a good model may be helpful also to identify critical nodes in the chain and help to improve its reliability by changing the topology of the supply chain network. In case when the inner structure of the system is unknown (for instance the concrete service strategy and other internal mechanisms) the modeling and identification can be performed only based on the available measurement input-output data, which means only black box like modeling and identification methods are utilized. In the literature many models (as for instance scheduling, transportation planning, flow-shop sequencing problem) related to logistic systems are based on the fuzzy set and fuzzy control theory, statistics or their combination [4][5][6][7][8][9].

During our previous studies we have investigated state space models together with subspace based identification to model and identify supply chains or loading systems and characterize the dependency between its certain factors [10]. A framework to promote the better understanding of supply chain performance measurement and metrics can be followed for example in [11]. In this paper let us focus on the impact of delays on the accuracy of the identified model by considering state space models and subspace identification techniques.

Many times it is difficult to find a proper mathematical model which would suitable approximate the behavior of the observed logistical process even if the identification of the system is considered locally. However subspace identification techniques combined with tensor product transformation seem to be promising to model complex logistical processes based on input-output data. In this case there is no need for an explicit model parametrization, which is a rather complicated matter for multi-output linear systems [12]. Based on given input-output pairs (which provide useful information about the unknown system) the discrete time, linear, time-invariant state space model of a logistical system (see later in section 3) will be identified by using subspace techniques.

Depending on the knowledge about the modeled system a broad range of solutions can be utilized. Since complex logistical systems are non-linear MIMO systems and are influenced by many parameters their modeling is not a trivial task. Many methods have been proposed to deal with multi-input, multi-output systems in the literature. Perhaps the most popular tool in this topic is the linear parameter varying (LPV) structure by which non-linear systems can be modeled and controlled on the basis of linear control theories. Furthermore, the most recent results of the numerical algebra, such as the higher order singular value decomposition and the related tensor product transformation (making connection between LPV models and higher order tensors) offer promising tools to bridge heuristic and analytic approaches. In such a joint framework besides analytic description of the system the expert knowledge can be considered, as well. This may further improve the effectiveness and extend the applicability of the related methods [13]-[16].

The paper is organized as follows: Section 2 gives a brief overview of subspace identification for deterministic case. In Section 3.1 and 3.2 examples are reported showing the effect of delays in supply chains on the accuracy of the identified model. Finally conclusions are reported.

## 2. Overview on Subspace Identification of LTI Systems

Before turning the focus onto modeling loading systems and related delays, let us give a brief description on how subspace identification techniques may be used to identify linear time invariant (LTI) vertex models in the parameter space. Let us assume that the local behavior of the logistical system is deterministic, thus it can be described in the well known state space form as follows:

$$\mathbf{x}_{k+1} = \mathbf{A}\mathbf{x}_k + \mathbf{B}\mathbf{u}_k \quad (1)$$

$$\mathbf{y}_k = \mathbf{C}\mathbf{x}_k + \mathbf{D}\mathbf{u}_k, \quad (2)$$

where  $\mathbf{x}_k \in \mathbb{R}^n$  stands for the state vector,  $\mathbf{u}_k$  and  $\mathbf{y}_k$  represent the input and output vector respectively at time  $kT$ , where  $T$  stands for the sampling time. The goal is to find the model matrices  $\mathbf{A}$ ,  $\mathbf{B}$ ,  $\mathbf{C}$  and  $\mathbf{D}$  based on input-output pairs. As described in [17] let us first arrange the input-output pairs into so called Hankel matrices (reflecting the history of our input-output data):

$$\mathbf{U}_{1|i} = \begin{bmatrix} \mathbf{u}_1 & \mathbf{u}_2 & \dots & \mathbf{u}_j \\ \mathbf{u}_2 & \mathbf{u}_3 & \dots & \mathbf{u}_{j-1} \\ \vdots & \vdots & \dots & \vdots \\ \mathbf{u}_i & \mathbf{u}_{i+1} & \dots & \mathbf{u}_{j+i-1} \end{bmatrix}, \quad (3)$$

$$\mathbf{Y}_{1|i} = \begin{bmatrix} \mathbf{y}_1 & \mathbf{y}_2 & \dots & \mathbf{y}_j \\ \mathbf{y}_2 & \mathbf{y}_3 & \dots & \mathbf{y}_{j-1} \\ \vdots & \vdots & \dots & \vdots \\ \mathbf{y}_i & \mathbf{y}_{i+1} & \dots & \mathbf{y}_{j+i-1} \end{bmatrix}, \quad (4)$$

where,  $i$  stands for the number of block rows (should be selected to be larger than the maximum order  $n$  of the system) and  $j$  denotes the number of columns, which in case of using all data samples is equal to  $N - i$ , where  $N$  represents the number of all input-output samples. Furthermore, let the history of states (unknown) to be estimated encode as follows:

$$\mathbf{X}_i = [\mathbf{x}_i \quad \mathbf{x}_{i+1} \quad \dots \quad \mathbf{x}_{i+j-1}]. \quad (5)$$

It can be recognized from (2) that all row vectors in  $\mathbf{Y}_{1|i}$  are in the vector space determined by the union of row space of  $\mathbf{X}_i$  and  $\mathbf{U}_{1|i}$ . Let us assume that the intersection of row space of  $\mathbf{X}_i$  and  $\mathbf{U}_{1|i}$  is empty. The most simple alternative for estimating  $\mathbf{X}_i$  (up to a constant multiple  $\mathbf{C}$ ) is to project the row space of  $\mathbf{Y}_i$  onto orthogonal complement of the row space of  $\mathbf{U}_{1|i}$ . The elements of  $\mathbf{Y}_i$  can be expressed with the help of the extended observability matrix  $\mathbf{\Gamma}_i$  and lower block triangular Toeplitz matrix  $\mathbf{H}_i$  form as follows [17]:

$$\mathbf{Y}_{1|i} = \mathbf{\Gamma}_i \mathbf{X}_1 + \mathbf{H}_i \mathbf{U}_{1|i}, \quad (6)$$

where

$$\mathbf{\Gamma}_i = [\mathbf{C} \quad \mathbf{CA} \quad \dots \quad \mathbf{CA}^{i-1}]^\top \quad (7)$$

and

$$\mathbf{H}_i = \begin{bmatrix} \mathbf{D} & 0 & 0 & \dots & 0 \\ \mathbf{CB} & \mathbf{D} & 0 & \dots & 0 \\ \mathbf{CAB} & \mathbf{CB} & \mathbf{D} & \dots & 0 \\ \mathbf{CA}^{i-2}\mathbf{B} & \mathbf{CA}^{i-3}\mathbf{B} & \dots & \mathbf{CB} & \mathbf{D} \end{bmatrix}. \quad (8)$$

By substituting recursively into (1) we can express the state sequence  $\mathbf{X}_{i+1}$  as follows:

$$\mathbf{X}_{i+1} = \mathbf{A}^i \mathbf{X}_1 + \mathbf{\Delta}_i \mathbf{U}_{1|i}, \quad (9)$$

where

$$\mathbf{\Delta}_i = [\mathbf{A}^{i-1}\mathbf{B} \quad \mathbf{A}^{i-2}\mathbf{B} \quad \dots \quad \mathbf{AB} \quad \mathbf{B}] \quad (10)$$

stands for the reversed extended controllability matrix [17]. From (6) the state sequence  $\mathbf{X}_1$  can be expressed as:

$$\mathbf{X}_1 = \mathbf{\Gamma}_i^* \mathbf{Y}_{1|i} - \mathbf{\Gamma}_i^* \mathbf{H}_i \mathbf{U}_{1|i}, \quad (11)$$

where \* denotes conjugate transpose of the matrix. By substituting (11) into (9) we obtain:

$$\mathbf{X}_{i+1} = \mathbf{A}^i \mathbf{\Gamma}_i^* \mathbf{Y}_{1|i} - \mathbf{A}^i \mathbf{\Gamma}_i^* \mathbf{H}_i \mathbf{U}_{1|i} + \mathbf{\Delta}_i \mathbf{U}_{1|i}. \quad (12)$$

Let us express  $\mathbf{X}_{i+1}$  as the sum of two matrices, where one of the matrices contains only the input-output values, i.e.

$$\mathbf{X}_{i+1} = \mathbf{L}_i \mathbf{W}_{1|i}, \quad (13)$$

where

$$\mathbf{L}_i = [\mathbf{\Delta}_i - \mathbf{A}^i \mathbf{\Gamma}_i^* \mathbf{H}_i \quad \mathbf{A}^i \mathbf{\Gamma}_i^*] \quad (14)$$

and

$$\mathbf{W}_{1|i} = [\mathbf{U}_{1|i} \quad \mathbf{Y}_{1|i}]^\top. \quad (15)$$

Since based on (6)

$$\mathbf{Y}_{i+1|2i} = \mathbf{\Gamma}_i \mathbf{X}_{i+1} + \mathbf{H}_i \mathbf{U}_{i+1|2i} = \mathbf{\Gamma}_i \mathbf{L}_i \mathbf{W}_{1|i} + \mathbf{H}_i \mathbf{U}_{i+1|2i}. \quad (16)$$

Let us now project  $\mathbf{Y}_{i+1|2i}$  onto orthogonal complement of  $\mathbf{U}_{i+1|2i}$ . Since the projection of  $\mathbf{H}_i \mathbf{U}_{i+1|2i}$  onto its orthogonal complement is empty subspace we obtain [17]:

$$\mathbf{Y}_{i+1,2i}/\mathbf{U}_{i+1,2i}^\perp = \mathbf{\Gamma}_i \mathbf{L}_i \mathbf{W}_{1|i}/\mathbf{U}_{i+1,2i}^\perp \quad (17)$$

$$(\mathbf{Y}_{i+1,2i}/\mathbf{U}_{i+1,2i}^\perp)(\mathbf{W}_{1|i}/\mathbf{U}_{i+1,2i}^\perp)^{-1} = \mathbf{\Gamma}_i \mathbf{L}_i, \quad (18)$$

$$\underbrace{(\mathbf{Y}_{i+1,2i}/\mathbf{U}_{i+1,2i}^\perp)(\mathbf{W}_{1|i}/\mathbf{U}_{i+1,2i}^\perp)^{-1}}_{\mathbf{O}_{i+1}} \mathbf{W}_{1|i} = \mathbf{\Gamma}_i \underbrace{\mathbf{L}_i \mathbf{W}_{1|i}}_{\mathbf{X}_{i+1}}, \quad (19)$$

$$\mathbf{O}_{i+1} = \mathbf{\Gamma}_i \mathbf{X}_{i+1} \quad (20)$$

where  $\mathbf{U}^\perp$  denotes the orthogonal complement of the row space of  $\mathbf{U}$ . Let us investigate the structure of  $\mathbf{O}_{i+1}$ . Based on (7) and (5) it can be expressed as:

$$\mathbf{O}_{i+1} = [\mathbf{C} \quad \mathbf{C}\mathbf{A} \quad \dots \quad \mathbf{C}\mathbf{A}^{i-1}]^\top [\mathbf{x}_{i+1} \quad \mathbf{x}_{i+2} \quad \dots \quad \mathbf{x}_{i+j}]. \quad (21)$$

Based on (21) the rank of  $\mathbf{O}_{i+1}$  equals to the rank of the state sequence matrix  $\mathbf{X}_{i+1}$ . Equivalently, the dimensionality of the state vector  $\mathbf{x}$  equals to the dimensionality of  $\mathbf{O}_{i+1}$ . The rank of  $\mathbf{O}_{i+1}$  can be determined by singular value decomposition (SVD) as follows[17]:

$$\mathbf{O}_{i+1} = \mathbf{U}_1 \mathbf{S}_1 \mathbf{V}_1 \quad (22)$$

$$\mathbf{\Gamma}_i \mathbf{X}_{i+1} = \mathbf{U}_1 \mathbf{S}_1^{1/2} \mathbf{T} \mathbf{T}^{-1} \mathbf{S}_1^{1/2} \mathbf{V}_1, \quad (23)$$

where  $\mathbf{T}$  is an arbitrary invertible square matrix representing a similarity transformation.

$$\mathbf{X}_{i+1} = \mathbf{T}^{-1} \mathbf{S}_1^{1/2} \mathbf{V}_1 \quad (24)$$

$$\tilde{\mathbf{X}}_{i+1} = \mathbf{S}_1^{1/2} \mathbf{V}_1 \quad (25)$$

The system matrix can be estimated in the least squares sense from the following set of equations:

$$\begin{bmatrix} \tilde{\mathbf{X}}_{i+2} \\ \tilde{\mathbf{Y}}_{i+1} \end{bmatrix} = \begin{bmatrix} \tilde{\mathbf{A}} & \tilde{\mathbf{B}} \\ \tilde{\mathbf{C}} & \tilde{\mathbf{D}} \end{bmatrix} \begin{bmatrix} \tilde{\mathbf{X}}_{i+1} \\ \tilde{\mathbf{U}}_{i+1} \end{bmatrix}, \quad (26)$$

where  $\mathbf{U}_{i+1}$  and  $\mathbf{Y}_{i+1}$  are input and output block Hankel matrices, respectively having one block row.

### 3. Modeling Supply Chains on Subspace Basis

In this section let us show through examples how supply chains can be modeled and identified on subspace bases. Furthermore let us also show through examples how the response times in the supply chain influence the identified model. The simulations have been performed by sampling interval  $T = 1[\text{sec}]$ .

### 3.1. Example 1

In this example transporting vehicles are loaded according to incoming demands in order to transport goods from warehouse located at A to a given destination B. To service a demand a free vehicle is needed to transport goods, loading machines are required to load the vehicle at A and unload it after its arrival at B. If the unloading process is completed the vehicle may return to the warehouse and wait for new incoming demands. The block diagram of the system used to generate simulation data can be seen in Fig. 1 while the parameters together with their actual values can be followed in Table 1.

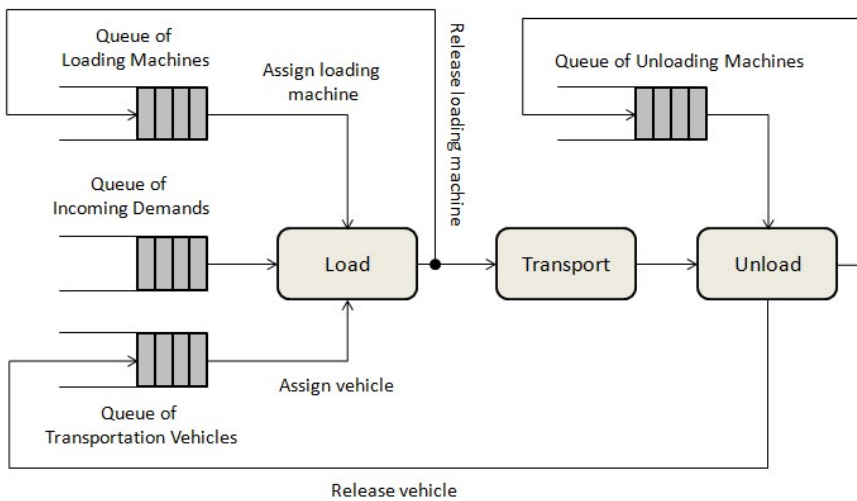


Figure 1. The architecture of the system designed to generate simulation data

Let us consider input-output pairs represented by the average waiting time of demands in the queue of demands as input  $u_1$  and the average service time of demands as output  $y_1$ . Let us identify the deterministic state space model describing the relationship between these two mentioned system parameters by using the above described subspace identification technique (see 2 for more details about subspace identification).

The input  $u_1$  can be followed in Fig. 2 while the corresponding simulated output (representing the measured data) together with the output of the estimated model are depicted in Fig. 3. The model estimation was performed based on 800 input-output data pairs. During the verification 1600 data pairs have been considered. The matrices of the identified state space model are as follows: The estimated system matrix:

Table 1. Setup of system parameters to generate simulation data

Parameter	Value
Number of loading machines	10
Number of vehicles	10
Number of unloading machines	3
Queue length of loading machines	40
Queue length of unloading machines	40
Queue length of vehicles waiting for loading	40
Queue length of incoming demands	50
Queue length of arrived vehicles	40
Loading time	Exponential distribution with mean 10
Unloading time	Exponential distribution with mean 10
Transport time	Exponential distribution with mean 10
Return time of vehicles	Exponential distribution with mean 10
Incoming rate of demands	Exponential distribution with mean 1

$$\mathbf{A} = \begin{bmatrix} 0.65029 & -0.1937 & 0.28359 & 0.17257 & -0.17277 & -0.0097291 & 0.078612 \\ -0.3566 & 0.68973 & 0.29488 & 0.36481 & -0.2482 & -0.064809 & 0.098057 \\ -0.36349 & -0.39037 & -0.27047 & 0.34423 & 0.22771 & -0.17696 & 0.055399 \\ 0.038496 & -0.11669 & -0.57838 & -0.13653 & -0.8574 & -0.42366 & -0.21459 \\ 0.15813 & 0.31372 & -0.25643 & 0.21981 & 0.28052 & -0.52284 & -0.11093 \\ 0.094546 & -0.23733 & 0.00031895 & 0.43292 & 0.068304 & -0.35473 & -0.5905 \\ -0.082549 & -0.0076265 & 0.29503 & -0.21588 & 0.042108 & -0.28678 & -0.61157 \end{bmatrix}$$

The estimated input matrix:

$$\mathbf{B} = [-0.17348 \quad -0.33904 \quad -1.1252 \quad 2.1473 \quad 0.78504 \quad 2.2637 \quad 4.2016]^T$$

The estimated output matrix:

$$\mathbf{C} = [39.62 \quad -9.8396 \quad 2.9335 \quad 1.5995 \quad -3.1529 \quad 3.2417 \quad -0.16641]$$

The initial state of the estimated system:

$$\mathbf{X}(0) = [12.427 \quad 23.417 \quad 82.997 \quad -155.83 \quad -74.708 \quad -170.02 \quad -361.04]^T$$

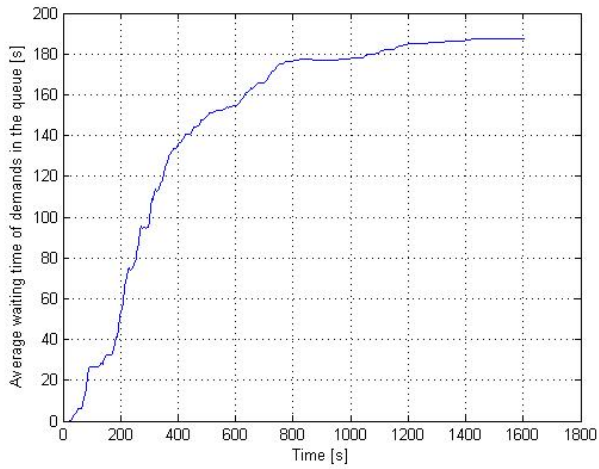


Figure 2. Input: average waiting time of demands in the queue of demands

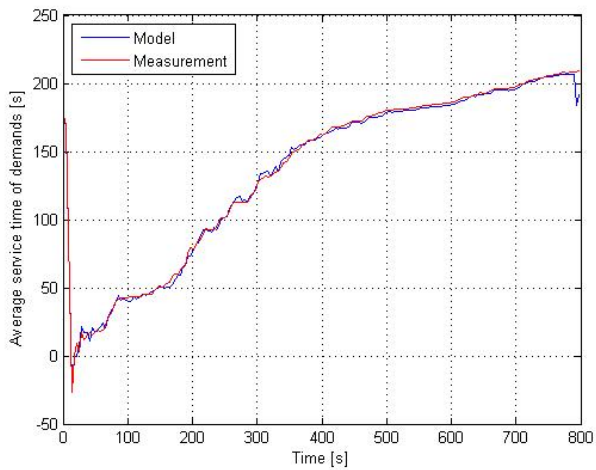


Figure 3. Output of the estimated model. Among 1600 input-output pairs 800 were used for model estimation.

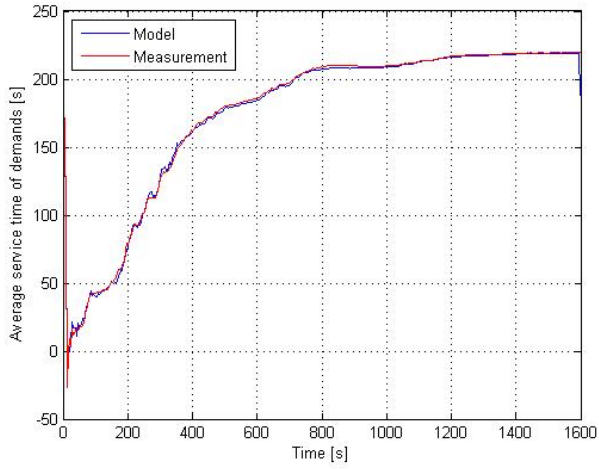


Figure 4. Validation of the estimated model. 1600 input-output pairs were used for validation.

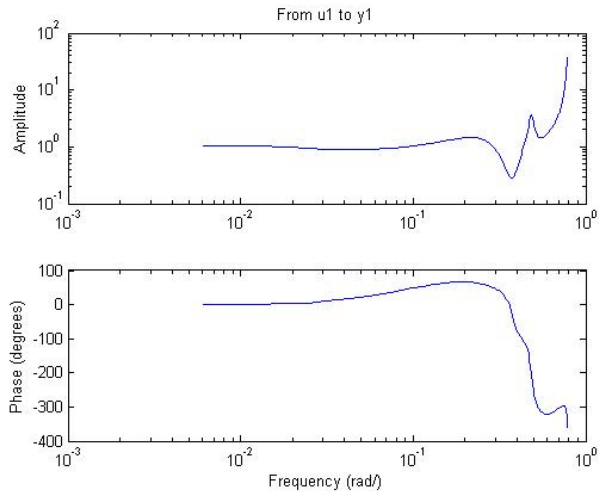


Figure 5. Bode plot of the identified model.

The response of the identified model clearly follows the required characteristics (see

Fig. 3). The verification of the estimated model has been performed by using 1600 data pairs among which the first 800 has been used for model estimation. The model clearly follows the measured output (see Fig. 4). The frequency response of the system can be followed in Fig. 5. As shown in the next example, the efficiency of identification of queuing systems on subspace basis is strongly influenced by delays present in the system.

### 3.2. Example 2

This example is aimed to show the influence of response time on the accuracy of the identified model. The architecture of the system used in this example is the same as in Example 1. However in contrast to the previous example here the transport time of goods have been doubled, while the number of transportation vehicles was significantly decreased in order to cause longer response times in the system (see Table 2).

The input represented by the average waiting time of demands in the queue of incoming demands can be followed in Fig. 6. The output represented by the average response time together with the response of the estimated model can be followed in Fig. 7. Finally the verification of the model is shown by Fig. 8. Compared to the previous example here the identification yielded a less accurate model (the cause is related to longer waiting times in the system). Although oscillations can be observed, the main characteristics of the measurement is clearly followed by the response of the estimated model. The matrices of the identified state space model are as follows: The estimated system matrix is:

$$A = \begin{bmatrix} 0.84984 & 0.10055 & 0.20797 & -0.1294 & 0.17411 & -0.0036611 & 0.022475 & -0.21601 \\ -0.38785 & 0.2428 & -0.018592 & -0.35352 & 0.63397 & 0.001635 & -0.056575 & -0.50946 \\ 0.1157 & 0.24374 & 0.21441 & 0.1744 & 0.66165 & 0.27477 & -0.52125 & 0.2711 \\ 0.031104 & 1.0741 & -0.085068 & 0.032735 & -0.7941 & 0.14308 & 0.12814 & 0.18568 \\ 0.20192 & 0.079581 & -0.67947 & -0.1361 & 0.35766 & -0.11025 & 0.18476 & 0.54493 \\ -0.042457 & -0.38714 & 0.10683 & -0.092881 & -0.14477 & 0.69397 & -0.11695 & 0.16482 \\ -0.013259 & 0.072086 & 0.11943 & 0.046148 & 0.1385 & 0.41882 & 0.77311 & 0.076762 \\ 0.13265 & 0.092821 & -0.26987 & -0.31781 & -0.15004 & 0.095917 & 0.012899 & -0.24774 \end{bmatrix}$$

The estimated input matrix is:

$$B = [-0.075538 \quad -0.02332 \quad 0.3248 \quad -0.49781 \quad -0.023601 \quad -0.1238 \quad 0.037839 \quad 0.12997]^T$$

The estimated output matrix:

$$C = [43.295 \quad -11.965 \quad 21.147 \quad -0.91197 \quad 5.812 \quad 36.454 \quad 19.316 \quad 7.3207]$$

The initial state of the estimated system:

$$X(0) = [-2.2054 \quad 27.437 \quad 27.061 \quad -70.7 \quad -22.441 \quad -17.067 \quad 1.1072 \quad 70.364]^T$$

Table 2. Setup of system parameters to generate simulation data

Parameter	Value
Number of loading machines	10
Number of vehicles	2
Number of unloading machines	3
Queue length of loading machines	40
Queue length of unloading machines	40
Queue length of vehicles waiting for loading	40
Queue length of incoming demands	50
Queue length of arrived vehicles	40
Loading time	Exponential distribution with mean 10
Unloading time	Exponential distribution with mean 10
Transport time	Exponential distribution with mean 20
Return time of vehicles	Exponential distribution with mean 10
Incoming rate of demands	Exponential distribution with mean 1

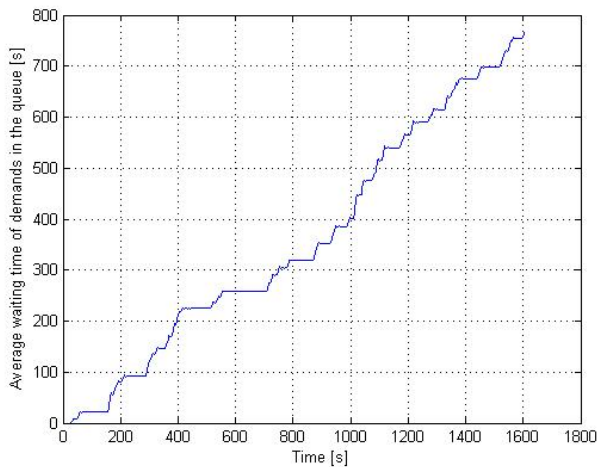


Figure 6. Input: average waiting time of demands in the queue of demands

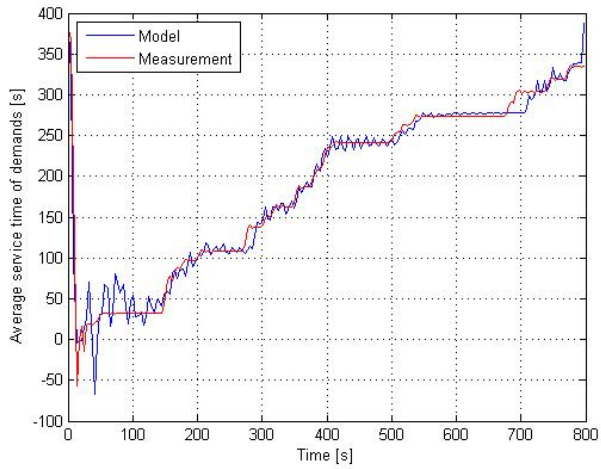


Figure 7. Output of the estimated model. Among 1600 input-output pairs 800 were used for model estimation.

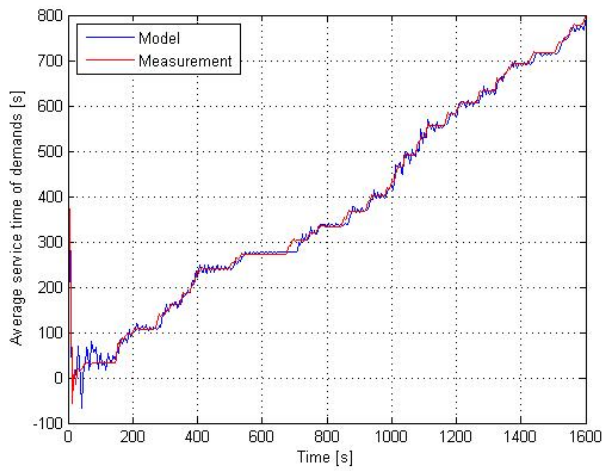


Figure 8. Validation of the estimated model. 1600 input-output pairs were used for validation.

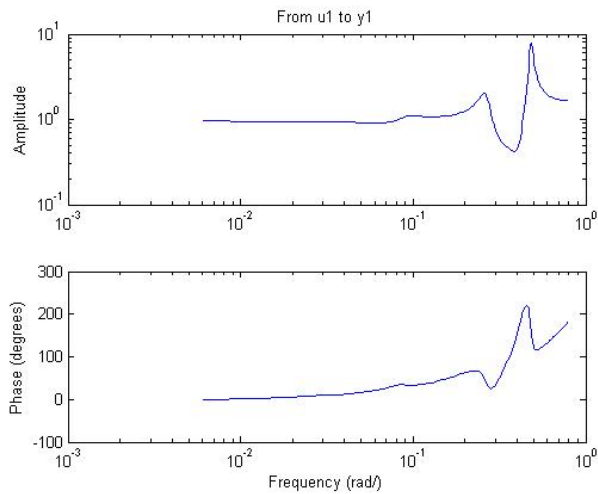


Figure 9. Bode plot of the identified model.

It can be recognized that the accuracy of the identified model is negatively affected by longer response times (compared to the previous example) in the queuing system. This inaccuracy appears in form of oscillations along the main characteristics of the system response (see Fig. 7). However the main characteristic of the model response are kept close to the measured one, thus crucial delays in the system may be detected even by evaluating the response of the identified model. The verification of the estimated model has been performed by using 1600 data pairs among which the first 800 has been used for model estimation. The main characteristics of the model clearly follows the measured output (see Fig. 8). The frequency response of the system can be followed in Fig. 9.

#### 4. Conclusions

During our previous studies we have investigated state space models and subspace identification to model and identify supply chains or loading systems as well as to characterize the dependency between its certain factors. In this paper we have turned the focus on the impact of delays on the accuracy of the identified model. Through simulations it was shown that increasing the delays in the system causes oscillations along the main characteristics of the estimated response. The loading systems have been modeled by discrete time, linear, time-invariant state space models and identified on subspace basis. The input-output data used for identification have been generated by a simulated loading system implemented in Matlab Simulink framework.

## References

- [1] K. Tang, C. Yang and J. Yang, “A Supply Chain Network Design Model for Deteriorating Items,” *International Conference on Computational Intelligence and Security*, Harbin, doi: 10.1109/CIS.2007.140, pp. 1020–1024, 2007.
- [2] H. L. Yin, “A New Method for Supply Chain Optimization with Facility Fail Risks,” *9th International Conference on Computational Intelligence and Security*, Leshan, doi: 10.1109/CIS.2013.81, pp. 353–357, 2013.
- [3] V. Bhaskar, P. Lallement, “Modeling a Supply Chain Using a Network of Queues,” *Applied Mathematical Modelling*, Vol. 34, Issue 8, ISSN 0307-904X, <http://dx.doi.org/10.1016/j.apm.2009.10.019>, pp. 2074–2088, August 2010.
- [4] I. Harmati, G. Orbán, P. Várlaki, “Takagi-Sugeno Fuzzy Control Models for Large Scale Logistics Systems, ” *Proc. Computational Intelligence and Intelligent Informatics International Symposium (ISCIII 07)*, Marocco, Agadir, doi: 10.1109/ISCIII.2007.367389, pp. 199–203, March 2007.
- [5] G. Orbán, P. Várlaki, “Fuzzy Modelling for Service Strategy and Operational Control of Loading Systems, ” *Acta Technica Jaurinensis, Series Logistica*, Vol. 2, No. 3, Published by Széchenyi István University, Faculty of Engineering Sciences, ISSN 1789-6932, pp. 375–391, 2009.
- [6] I.Á Harmati, L.T. Kóczy, “On the Sensitivity of Weighted General Mean Based Type-2 Fuzzy Signatures, ” *In: Rutkowski L., Korytkowski M., Scherer R., Tadeusiewicz R., Zadeh L., Zurada J. (eds) Artificial Intelligence and Soft Computing. ICAISC 2016. Lecture Notes in Computer Science*, doi:10.1007/978-3-319-39378-0\_19, pp. 206–218, June 12–16, 2016.
- [7] I.Á Harmati, L.T. Kóczy, “On the Sensitivity of Type-2 Fuzzy Signatures and the Generalizations of the Extension Principle, ” *2016 IEEE International Conference on Fuzzy Systems*, Vancouver, BC, doi:10.1109/FUZZ-IEEE.2016.7737839, pp. 1301–1307, July 24–29, 2016.
- [8] Jing-Shing Yao, Feng-Tse Lin, “Constructing a Fuzzy Flow-Shop Sequencing Model Based on Statistical Data, ” *International Journal of Approximate Reasoning*, Vol. 29, Issue 3, ISSN 0888-613X, doi:10.1016/S0888-613X(01)00064-0, pp. 215–234, March 2002.
- [9] P.V. Sevastjanov, P. Róg, “Fuzzy Modeling of Manufacturing and Logistic Systems,” *Mathematics and Computers in Simulation*, Vol. 63, Issue 6, ISSN 0378-4754, doi:10.1016/S0378-4754(03)00064-8, pp. 569–585, 24 November 2003.
- [10] T. Vadvári, P. Várlaki, “Queuing Models and Subspace Identification in Logistics,” *Acta Technica Jaurinensis*, Vol. 8, No. 1, pp. 63–76, 2015.

- [11] A. Gunasekaran, C. Patel, Ronald E. McGaughey, “A Framework for Supply Chain Performance Measurement,”*International Journal of Production Economics*, Vol. 87, Issue 3, ISSN 0925-5273, doi:10.1016/j.ijpe.2003.08.003, pp. 333–347, 18 February 2004.
- [12] Peter Van Overschee, Bart De Moor, “Subspace Identification for Linear Systems, Theory - Implementation - Applications, ”*Kluwer Academic Publishers*, Boston/London/Dordrecht, ISBN: 978-1461380610, p. 272, 2011.
- [13] L. Szeidl, P. Baranyi, Z. Petres, and P. Várlaki, “Numerical Reconstruction of the HOSVD Based Canonical Form of Polytopic Dynamic Models,”*3rd International Symposium on Computational Intelligence and Intelligent Informatics*, Agadir, Morocco, doi:10.1109/INES.2006.1689368, pp. 111–116, 2007.
- [14] S. Nagy, Z. Petres, and P. Baranyi, “TP Tool-a MATLAB Toolbox for TP Model Transformation ”in *Proc. of 8th International Symposium of Hungarian Researchers on Computational Intelligence and Informatics*, Budapest, Hungary, pp. 483–495, 2007.
- [15] P. Baranyi, Z. Petres, P. Korondi, Y. Yam, H. Hashimoto, “Complexity Relaxation of the Tensor Product Model Transformation for Higher Dimensional Problems,”*Asian Journal of Control*, Vol. 9, No. 2, pp. 195–200, 2007, doi: 10.1111/j.1934-6093.2007.tb00323.x
- [16] P. Baranyi, D. Tikk, Y. Yam, R. J. Patton, “From Differential Equations to PDC Controller Design via Numerical Transformation,”*Computers in Industry*, Vol. 51, No. 3, doi:10.1016/S0166-3615(03)00058-7, pp. 281–297, 2003.
- [17] P. van Overschee, B.L. de Moor, “Subspace Identification for Linear Systems: Theory - Implementation - Applications, ”*Springer*, Softcover reprint of the original 1st ed. 1996 edition, October 8, 2011.

# Creating a two-way Land-Use and Transport Interaction model for Budapest

M. Juhász<sup>1</sup>, Cs. Koren<sup>1</sup>

<sup>1</sup> Széchenyi István University, Department of Transport Infrastructure  
Egyetem tér 1, 9028 Győr, Hungary  
Phone: +36 20 233 3318  
e-mail: mjuhasz@sze.hu

**Abstract:** This paper intends to show that despite limited data availability it is still possible to elaborate semi-sophisticated LUTI models which can be a stepping stone for countries that are less developed in terms of transport modelling practice but eager to improve. It provides an outline of the model and of the calibrating process which was based on data from the city of Budapest. Based on the results it is undeniable that excluding land-use effects of transport in modelling could cause a serious distortion even in a shorter time period. It seems that such land-use effects and feedbacks can no longer be disregarded as it is not in accordance with the desire of improving transport modelling practice. From this aspect, the proposed approach is practical and can overcome general obstacles of time, cost and data availability issues. The next step should be to carry out tests for the estimation of real transport investments and compare the results with other models.

**Keywords:** *land-use and transport interaction, modelling, urban transport, calibration*

## 1. Introduction

Urban transport planning was mainly dominated by supply generative interventions in the second part of the last century and for most of the time car users were the beneficiaries. Approaching the turn of the millennium transport planning principles were about to change and the so-called principle of ‘predict and provide’ has been continuously replaced by ‘aim and manage’. Nowadays urban transport planning is about to find the balance and the optimal solution in providing space and possibilities for different transport modes. Naturally and due to the “heritage” of the previous era, it involves the conflicting action to break the dominance of private cars besides the provision and promotion of different alternatives. In doing so it is going to be more and more crucial for policy- and decision makers to be able to recognize and assess all possible effects, consequences and scenarios. That is not only to increase transparency, public acceptance and to ensure accountability, but it comes with the responsibility to impose different “game-changing” acts upon travellers or to spend significant amounts of investment on infrastructure which could shape city structure and influence several aspects of life. [1-5]

Technical advances make it possible to create more and more accurate models of social and economic systems. With the emergence of these models, transport interactions, policies and strategies can be tested before implementation. That can aid the decision-making process in order to choose the best possible option, fine-tune solutions and also to prevent or minimize undesirable side-effects. Such analyses can be crucial as some interventions (e.g. the calming of road traffic) implemented in an inappropriate way may hinder economic competitiveness or lead to mass residential migration away. For instance, in the case of the city of Budapest three major traffic calming schemes have been abandoned in the last couple of years due to the significant amount of uncertainty and risk which were not possible to be adequately analysed in the absence of data and proper modelling tools [6]. [7-9]

The main set of issues with the prevailing practice in transport appraisal is that benefits arising from long-term impacts on land-use and economic activities are often ignored or remain hidden [10]. A role model that addressed those issues is the ULTrA (Unified Land-use/Transport Appraisal) approach from the UK which was developed based on the case of London and combined LUTI (Land-Use and Transport Interaction) modelling and transport appraisal methods. Based on this role model and its preliminaries (e.g. the DELTA LUTI modelling package), previous parts of this research also set up an assessment framework with a LUTI model in the centre of it (for details see: [6]).

The objective of this paper is to show that despite limited data availability it is still possible to elaborate semi-sophisticated LUTI models which can be a stepping stone for countries that are less developed in terms of transport modelling practice but eager to improve. The paper provides an outline of the model and of the calibrating process which was based on data from Budapest. It also intends to discuss the results obtained and the limitations of the model. It also summarizes the lessons learnt and draft further work.

## **2. Overview of the model**

The prototype of the LUTI model for Budapest was developed in 2015. The key intention and challenge in creating it was the simultaneous requirement to provide a certain level of quality compared to state-of-the-practice models and to lean on a reasonably limited set of data. The underlying concept was that leading models need a serious amount of data which is not available for cities in most countries and this fact restrains the practical application of them. Therefore it was intended to bypass this issue by model design. Another important aspect was that the model should be used within the previously mentioned assessment framework which means that its inputs and outputs should be compatible with those in the framework. [6]

The model was elaborated by the combination, modification and amendment of three previous models, namely the DELTA model from the UK [11], MARS model from Austria [12] and the TIGRIS XL model from the Netherlands [13]. It consists of three dynamically interconnected parts: a transport decision model, a land-use decision model and a population model. The first one estimates travel-related choices (number of trips per modes and routes) and their consequences (travel times and costs); the second model forecasts real-estate developments (number of houses to be built) and location choices of residents and businesses; while the third deals with ageing. The essential links between the transport and the land-use model are that travel times (and costs) estimated by the

transport model (as a result of the interaction between transport demand and supply) are used in the land-use model embedded in the endogenous variables of accessibility to influence land-use changes, while these changes are used in the transport model to generate transport demand [14]. In order to represent time lags and the evolution of the changes the model uses time steps of one year. So impacts of changes are emerging gradually over a number of years. Further details on the elaboration process, the origination and the concept of design can be found in [6].

This paper focuses on the description of model elements (modules) to provide background for the calibration process. The structure and main relationships of the modules in one time period are illustrated by Fig. 1. Note that the study area is represented by zones as it is common in transport modelling. The model always simulates a base year and forecasts changes on that platform. One can also note that there are some changes in the scope and workings of the model compared to the prototype. These were all inevitable due to data availability during the calibration and will be described and discussed later on in the paper.

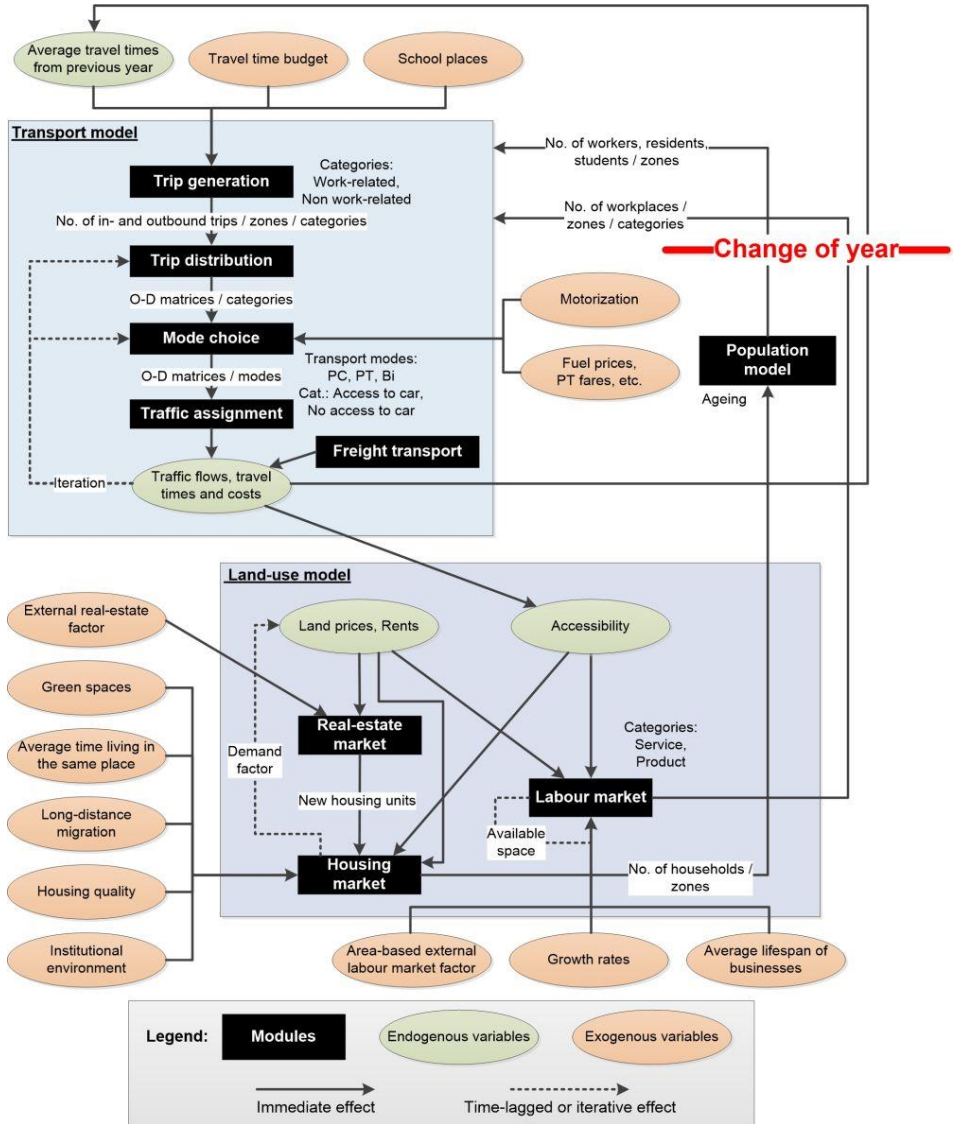


Figure 1: The overview of the LUTI model

### Trip-generation

Each year starts with the trip generation module which calculates the number of trips induced within the modelling area. Two types of trips are considered in the model: work-related (WR) and non-work-related (NWR) trips. Daily outbound (production) and inbound (attraction) trips for each zone are calculated based on the following equations (1)-(7):

$$Prod_i = aR_i + bW_i + cS_i + ceSP_i + (7a + bd)WPS_i + bdWPP_i \quad (1)$$

$$Attr_i = aR_i + bdW_i + ceS_i + cSP_i + (7a + b)WPS_i + bWPP_i \quad (2)$$

$$Prod_{WR,i} = bW_i + cS_i + ceSP_i + bd(WPS_i + WPP_i) \quad (3)$$

$$Attr_{WR,i} = bdW_i + ceS_i + cSP_i + b(WPS_i + WPP_i) \quad (4)$$

$$Prod_{NWR,i} = Prod_i - Prod_{WR,i} \quad (5)$$

$$Attr_{NWR,i} = Attr_i - Attr_{WR,i} \quad (6)$$

$$a = \frac{TTB R^t - T_{WR}^{t-1} ATT_{WR}^{t-1}}{ATT_{NWR}^{t-1} (R^t + 7WPS^t)} \quad (7)$$

where:

- $Prod_{WR,i}$  and  $Attr_{NWR,i}$  are the work-related production and non-work-related attraction respectively for zone  $i$
- $R$ ,  $W$ ,  $S$ ,  $SP$ ,  $WPS$  and  $WPP$  are the number of residents, workers, students, school places, workplaces for services and workplaces for production respectively
- $TTB$  is the travel time budget for an average resident (in mins)
- $T_{WR}^{t-1}$  is the number of total work-related trips in the previous year (time period  $t-1$ )
- $ATT$  is the average travel time (in mins)
- $b$ ,  $c$ ,  $d$  and  $e$  are constant parameters to be calibrated ( $a$  is also a parameter, but can be calculated)

Please note that the attraction values need a correction in order to ensure that its sum equals to the sum of production.

### Trip-distribution

Then the trip distribution module distributes the generated trips to origin-destination pairs using a doubly-constrained gravity method (for details see chapter 5.3 in [15]). The deterrence function of the model is disaggregated into travel time bins (ranges). The number of bins can be adjusted during calibration. Trip distribution equations are the following (8)-(10):

$$T_{ij} = A_i Prod_i B_j Attr_j f(WTT_{ij}) \quad (8)$$

$$f(WTT_{ij}) = \sum_k \exp(\beta_k WTT_{ij}) \delta_{ij}^k \quad (9)$$

$$WTT_{ij} = \sum_m w_{ij,m} tt_{ij,m} \quad (10)$$

where:

- $T_{ij}$  is the total number of trips between the origin-destination pair of zone  $i$  and  $j$
- $A_i$  and  $B_j$  are balancing factors in the iterative part of the doubly-constrained gravity model (for details see chapter 5.3 in [15])
- $f(WTT_{ij})$  is the deterrence function
- $WTT_{ij}$  is the weighted travel time between the origin-destination pair of zone  $i$  and  $j$  (in mins)
- $w_{ij,m}$  is the ratio of trips made by mode  $m$  between the origin-destination pair of zone  $i$  and  $j$
- $tt_{ij,m}$  is the travel time of mode  $m$  between the origin-destination pair of zone  $i$  and  $j$  (in mins)
- $\beta_k$  is a constant parameter for travel time bin  $k$  to be calibrated
- $\delta_k$  equals to 1 if the travel time between zone  $i$  and  $j$  falls in the travel time bin  $k$  and equals to 0 otherwise

### Mode-choice

Then in the mode-choice module the distributed trips are divided between modes. Three transport modes (private car, public transport and bicycle) are considered in the module. The probability that a trip is about to occur by a certain mode is based on a multinomial logit model taking into account the car availability of travellers according to the following method (equation (11)-(17)):

$$T_{c,ij,pc} = \sum_c T_{c,ij} CA_i \frac{Imp_{c,ij,pc}}{\sum_m Imp_{c,ij,m}} \text{ for } m = \begin{cases} pc \\ pt \\ bi \end{cases} \quad (11)$$

$$CA_i = COw_i COcc \quad (12)$$

$$T_{c,ij,pt} = \sum_c T_{c,ij} \frac{Imp_{c,ij,pt}}{\sum_m Imp_{c,ij,m}} \text{ for } m = \begin{cases} pt \\ bi \end{cases} \quad (13)$$

$$T_{ij,bi} = \sum_c T_{c,ij} \frac{Imp_{c,ij,bi}}{\sum_m Imp_{c,ij,m}} \text{ for } m = \begin{cases} pt \\ bi \end{cases} \quad (14)$$

$$Imp_{c,ij,pc} = \exp(a_{pc,c} + b_{pc,c} tt_{ij,pc} + c_{pc,c} pt_{ij} + d_{pc,c} \frac{rc_{ij}}{VOT_c} + e_{pc,c} \frac{VOC_{ij}}{VOT_c}) \quad (15)$$

$$Imp_{c,ij,pt} = \exp(a_{pt,c} + b_{pt,c} ivt_{ij} + c_{pt,c} cht_{ij} + d_{pt,c} wt_{ij,car} + e_{pt,c} \frac{PTF_{ij}}{VOT_c}) \quad (16)$$

$$Imp_{c,ij,bi} = \exp(a_{bi,c} + b_{bi,c} tt_{ij,bi}) geo_{ij} \quad (17)$$

where:

- $T_{c,ij,m}$  is the number of trips between zone  $i$  and  $j$  by mode  $m$  (modes:  $pc$  – private car,  $pt$  – public transport,  $bi$  – bicycle) for WR and NWR trips (the latter is indicated by subscript ‘c’)
- $Imp_{c,ij,m}$  is the impedance of a trip between zone  $i$  and  $j$  by mode  $m$  for WR and NWR trips
- $CA$ ,  $COw$ ,  $COcc$  is the car availability, car ownership (number of cars / 1000 residents) and car occupancy respectively

- $tt_{ij,pc}$  and  $tt_{ij,bi}$  is the (congested) travel time between zone  $i$  and  $j$  by cars and bicycles respectively (in mins)
- $pt$ ,  $rc$ ,  $VOC$  is the parking time, road charge (including parking fees) and vehicle operating cost respectively for private car trips (in mins and EUR)
- $ivt$ ,  $cht$ ,  $wt$  and  $PTF$  is the in-vehicle time, transfer time, origin waiting time and fare respectively for public transport trips (in mins and EUR)
- $geo$  is a geographical factor for bicycle trips (adopted from the official transport model for Budapest, see chapter 6 in [16])
- $a$ ,  $b$ ,  $c$ ,  $d$ ,  $e$  for different modes are constant parameters to be calibrated

Note that both trip distribution and mode choice models use the prevailing travel time values of the actual time period. It means that these modules have an iterative process to ensure that actual travel times are taken into account.

For freight transport there is a separated and simplified trip generation and distribution step. The former is generating traffic based on the number of workplaces for each category (services and production); while the latter is simply distribute the production based on the relative attractiveness of the zone compared to the sum of attractions.

### Traffic assignment

As a result of the aforementioned modules daily origin-destination matrices for each transport mode can be produced. Then these matrices are assigned to the transport network. In this case it is also done based on the official transport model for Budapest, which uses standard equilibrium assignment for private modes and headway-based assignment for public transport. Details about the assignment method and the parameters of the impedance function can be found in [16] (chapter 7.1).

### Intermediate calculations

Based on the results of the transport model (mainly “congested” travel times) the endogenous variable of accessibility can be calculated. Other endogenous variables can also be calculated based on the results of the land-use model from the previous time period. These calculations are the following (equation (18)-(21)):

$$Acc_i = \frac{\sum_j [(R_j + WPS_j + WPP_j) a WTT_{ij}]}{\sum_j (R_j + WPS_j + WPP_j)} \quad (18)$$

$$RT_i^t = RT_i^{t-1} (1 + b DF_i^{t-1c}) \quad (19)$$

$$LP_i^t = LP_i^{t-1} (1 + d DF_i^{t-1e}) \quad (20)$$

$$CB_i = LP_i + 100ABC \quad (21)$$

where:

- $Acc_i$  is the accessibility of zone  $i$
- $RT$  is a virtual rent rate which represents the value of a housing unit in EUR/m<sup>2</sup>/month

- DF is the demand factor for each zone from the housing market module (which is described later on)
- LP and CB is the land price and the cost of building respectively in EUR/100m<sup>2</sup>
- ABC is the average building cost of a m<sup>2</sup> in EUR
- a, b, c, d, e are constant scaling and elasticity parameters to be calibrated

### Real-estate market

Following the previous steps, based on some exogenous variables and the accessibility, changes in the land-use system are calculated. At first, the real-estate market module forecasts the number of new housing units to be built by zones. Initially, the unconstrained demand for building is calculated based on the expected weighted profitability. Profitability of a zone is the difference between the market value and the building cost of a residential m<sup>2</sup>. Weighting is done based on the value of existing residential floorspace. Then this demand is constrained as developers seek to retain a “development stock” [9]. The extent of actual development depends on the size of the demand relative to the total available space for building. Then the constrained demand is allocated to zones on the basis of relative expected profitability. The developed floorspace is then converted into number of housing units. If there is more demand for building than the available space in a certain zone, then that overflowing demand is not taken into consideration (it is a latent demand). The equations of the module are the following (22)-(24):

$$UncDB^t = a \sum_i FR_i^{t-1} \left( \frac{\sum_i (RT_i^t - CB_i^t) FR_i^{t-1}}{\sum_i FR_i^{t-1}} \right)^b \quad (22)$$

$$ConstDB^t = c \left( \frac{UncDB^t}{\sum_i AFR_i^{t-1}} \right)^d \quad (23)$$

$$NHU_i^t = \frac{ConstDB^t \frac{(RT_i^t - CB_i^t) FR_i^{t-1}}{\sum_i (RT_i^t - CB_i^t) FR_i^{t-1}}}{AHHS} \quad (24)$$

where:

- UncDB and ConstDB are the unconstrained and constrained demand for building in m<sup>2</sup>
- FR is the existing floorspace of residential buildings in m<sup>2</sup>
- AFR is the available floorspace for residential buildings in m<sup>2</sup>
- NHU is the number of new housing units to be built
- AHHS is the average household size in m<sup>2</sup>
- a, b, c, d are constant scaling and elasticity parameters to be calibrated

### Housing market

Next, in the housing market module location choices of residents (grouped to households) are estimated. At first, a “moving-out” equation calculates the number of households that are leaving their actual location based on an average time-span for living in the same place. As a result of the moving-out process there will be empty housing units above those which are already empty. These empty ones plus the new housing units

calculated by the real-estate market module give the total housing unit supply in a time period. Consequently the demand for housing units is the sum of the households that moved out and those who are moving into the study area from a longer-distance. The latter is calculated by a so-called “long-distance migration” factor. Please note that in the model every household lives in one housing unit. A “moving-in” equation distributes the constrained demand between zones based on zonal utility. Five factors are influencing the choices: housing quality, ratio of public green spaces, institutional environment, accessibility and the virtual rent rate. Within the utility function there is a correction factor for zone size as the number of out-movers depends on the size so the utility for in-movers also needs correction for that. The demand is constrained by the total number of available housing units. If there is an overflowing demand in a zone then it is re-distributed to the second best alternatives with available space. One can note that a household can move out from a certain zone and then move in again which would not mean a change in the number of households in that zone. The module consists of the following equations (25)-(31):

$$HHmo_i^t = \frac{HH_i^{t-1}}{ATSL} \quad (25)$$

$$HS_i^t = NHU_i^t + HHmo_i^t + (HS_i^{t-1} - HHmi_i^{t-1}) \quad (26)$$

$$HD^t = \sum_i HHmo_i^t + R^{t-1}LDM^t \quad (27)$$

$$HHmi_i = HD \frac{RU_i}{\sum_i RU_i} \quad (28)$$

$$RU_i = \exp(aAcc_i + bHQ_i + cGS_i + dINS_i + eRT_i + fUCFH_i) \quad (29)$$

$$UCFH_i = \frac{HH_i}{HH_i} \quad (30)$$

$$DF_i = \frac{HHmi_i}{HS_i} \quad (31)$$

where:

- $HH_{mo}$  and  $HH_{mi}$  is the number of households moving-out and moving-in, respectively
- $HS$  and  $HD$  are the housing supply and demand respectively
- $ATSL$  is the average time-span for living in the same place (in years)
- $LDM$  is a long-distance migration factor in % (positive if the number of residents is increasing in the study area)
- $RU$  is the utility for residents
- $HQ$ ,  $GS$ ,  $INS$  are the variables representing the housing quality, the ratio of public green spaces and the institutional environment (values between 0-10)
- $UCFH$  is the utility correction factor for zone size
- $a$ ,  $b$ ,  $c$ ,  $d$ ,  $e$  and  $f$  are constant parameters to be calibrated

## Labour market

The following is the labour market module which forecasts the location choices of businesses (represented by number of workplaces). The module considers two types of

business activities: services and production. It works similarly to the housing market module. First of all there is also a moving-out process based on the average life-span of businesses which means that a business is either moving to another location (outside the study area) or it is closing. As a result of the moving-out process some business floorspace will become unoccupied. The next step is to exogenously define the number of in-moving businesses which represents re-locating or newly developed ones. The zonal allocation of these workplaces is done based on a utility function which considers the cost of building (land prices), accessibility and an area-based external factor. The latter represents those utility aspects that are not included in the model. Similarly to the real-estate market module there is also a constrained development by available floorspace and just like in the housing market module, a correction factor for zone size is included. The equations of the module are the following (32)-(38):

$$WPmo_{i,c}^t = \frac{WP_{i,c}^{t-1}}{ALSB} \quad (32)$$

$$WPD_c^t = WP_c^{t-1} \cdot BGR^t \quad (33)$$

$$WPMi_{i,c} = WPD_c \cdot \frac{BU_{i,c}}{\sum_i BU_{i,c}} \quad (34)$$

$$BU_{i,c} = \exp(a_c \cdot Acc_i + b_c \cdot CB_i + c_c \cdot UCFB_{i,c} + ELMF_{i,c}) \quad (35)$$

$$UCFB_{i,c} = \frac{WP_{i,c}}{WP_{i,c}} \quad (36)$$

$$WPS_i = WP_{i,c} \quad \text{if } c = 1 \text{ (services)} \quad (37)$$

$$WPP_i = WP_{i,c} \quad \text{if } c = 2 \text{ (production)} \quad (38)$$

where:

$WP_{mo}$  and  $WP_{mi}$  is the number of businesses (workplaces) moving-out and moving-in respectively for service and production sector (the latter is indicated by subscript 'c')

WPD is the total number of workplaces “moving-in” (total demand)

ALSB is the average life-span of businesses (in years)

BGR is the business growth rate in %

BU is the utility for businesses

UCFB is the utility correction factor for zone size

ELMF is the external factor for utility components that are not involved

a, b, c are constant parameters to be calibrated for each category

### Demographic changes and feedback loops

Finally, the population module deals with demographic changes. It is modelling the ageing of the society using the following Markovian transition model of probabilities (Table 1).

Table 1: Probabilities of the Markovian transition model for demographic changes

States	Potential mother	0-15 year group	16-65 year group	65+ group	Deceased
Potential mother	1-a	a	0	0	0
0-15 year group	0	1-(b+c)	b	0	c
16-65 year group	0	0	1-(d+e)	d	e
65+ group	0	0	0	1-f	f
Deceased	0	0	0	0	1

The conversion between the number of residents and households is done by an average household size. There is another conversion between spaces and housing units and workplaces based on average sizes.

As a result of the population model, the number of residents, workers and students can be calculated based on ratios from previous years or on external changes. These values along with the number of workplaces, school places and average travel times provide input for the transport model to run another year (cyclic phase).

### 3. Calibration process

Previously, in the paper describing the structure of the model, there was a demonstration case to verify and check the operation of the model on a hypothetical scenario [6]. In this paper the objective is to calibrate model parameters on a real case. For that reason all relevant and available data were collected for the city of Budapest. An ideal calibration of the whole model would require actual (observed) data on transport and land-use decisions and disaggregate data on a large sample of travellers and households revealing the explanatory factors of their decisions. Data should be sufficiently precise to allocate them spatially (to zones) and to person or household groups. In spite of the fact that such stated- and revealed-preference data would be highly desirable, this researched faced many challenges to obtain the most needed parts of the dataset. It was previously highlighted that model design was also intended to handle some of these “lack of data” and “lack of disaggregation” problems to be able to provide a semi-sophisticated structure. However, these issues still affected the calibration process.

Due to the limitations of available data and constrains of this research on assembling new data, much of the calibration of the model has been based on existing, observable changes of dependent and explanatory variables. Unfortunately it led to some further simplification of the model, which also suggests handling the results with care. From that point the main objective was to calibrate each sub-system (module) separately for a time period for which all relevant data is available or there is a way to reliably replace or estimated them. Some data manipulation was also needed as for some variables either the aggregation level was not adequate or annual changes of values was not available.

First of all, as a starting point and a reference case, the official transport model of Budapest has been selected. That model was available for the year 2015 with a transport

demand part which was well-supplemented by household surveys. Relevant statistical data for Budapest (e.g. number of residents) was available between 2007 and 2014 from the Hungarian Central Statistical Office. Then, the time period from 2007 to 2013 has been chosen for the calibration of the land-use model in which changes usually require a longer time-span to evolve. It was also an influencing factor that the metro line M4 was opened in 2014 and it was intended to avoid its short-run disturbing effects. Therefore 2014 was used to calibrate the transport model based on the official one.

Secondly, the spatial system for the model had to be decided. It was evident that annual land-use data is only available for the district level (for 23 districts in Budapest). However, a proper transport model needed a higher resolution than that, so the sub-district level has been chosen as the zonal basis of the transport model (with 162 zones for the sub-districts). In order to model suburban areas in the region of Budapest, another 30 zones were set up as cordon zones. In the land-use model these were aggregated into 5 agglomeration zones. For an illustration see Fig. 2.

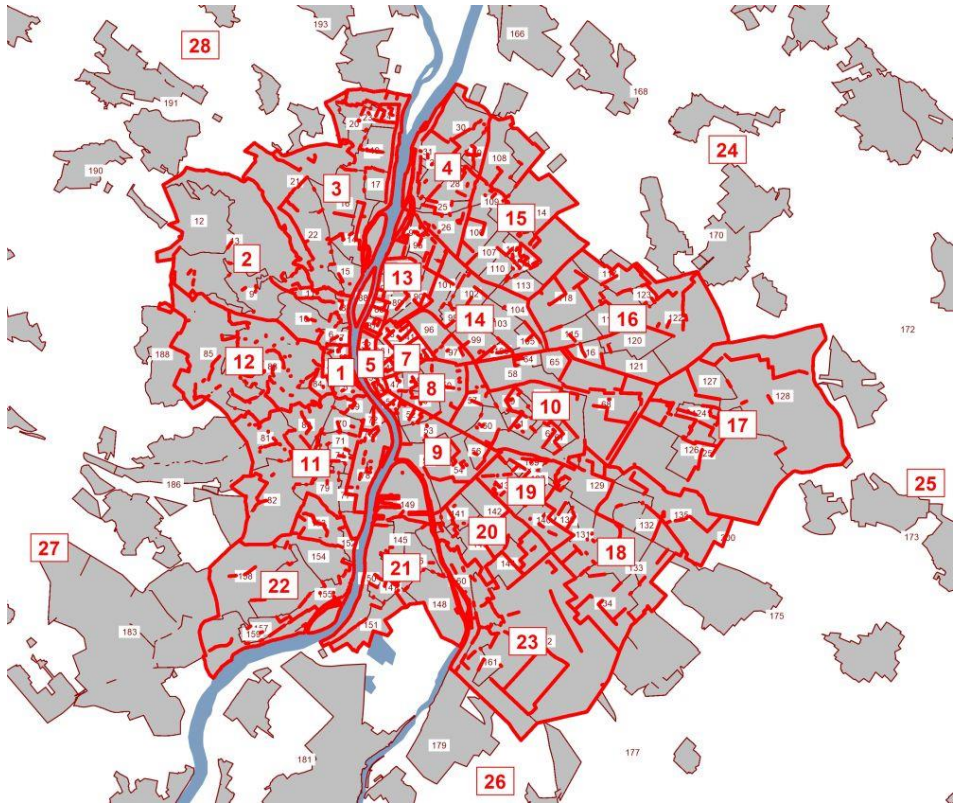


Figure 2: Zone system of the model (grey: transport zones – sub-districts, red: land-use zones - districts)

During the calibration of the transport model, the official network model of 2015 (with around 1200 zones) was used as a basis. This model was modified to represent the year of 2014 (there were some minor changes in the network and in public transport services).

Then transport zones were aggregated and their connectors were adjusted to create the modified model with 192 zones. Then it was needed to replicate the demand model in a synthetic way. It is important to note that the official model uses direct demand modelling and its matrices for the base year are originated that way. However, in its matrix forecasting method, the official model also uses a synthetic demand model combined with pivoting. In this research this synthetic demand model was replaced to be compatible with the land-use model. The calibration has been done for 2014 in each module. Trip generation module was calibrated in a way that its results (i.e. the sums of outbound and inbound trips for zones) approximate the sums of the direct matrices of the official model. Trip distribution module approximates the values of each cell, while mode-choice module tries the same for the direct matrices of each transport mode.

Since land-use model calculations require transport-related data (e.g. travel times) for each year between 2007 and 2013, transport models were needed to be produced for these years. Network models for these earlier years were created by stepping backwards from 2014. Considering the demand side, it was done by the calibrated transport-related modules based on the network states of each year. Matrices were calculated by using the pivoting method as quite naturally direct demand matrices cannot be properly approximated by synthetic models [15]. As a result transport-related values were calculated for the mentioned seven years.

Based on travel time values the explanatory variable of accessibility was calculated for the land-use model from 2007 to 2013. Values of other explanatory variables such as rents or housing quality indicators were available or calculated. The modules of the land-use model were calibrated in order to approximate the changes in the number of households, workplaces and new housing units. For the real-estate, housing and the labour market module the calibration was done for the entire time period taking into consideration the total change of the dependent variable. This issue comes from the nature of the real-estate and the housing market where there are hectic changes, while for the number of workplaces there was not data for exact annual changes. Endogenous variables of land prices and rents were calibrated normally for changes per annum (i.e. 6 years as the land-use changes of 2007 are not included). For real-estate market the agglomeration area has not been taken into account.

During the calibration of the location choice (housing and labour market) modules there was a technical challenge as only the changes in the number of households and workplaces were known from the available data. There was not a sample of “from-to” moves. Therefore the observed changes were artificially recreated in a moving-out and moving-in structure which is in line with the model design. Then the main focus was to explain the moving-in process with a multinomial logit model and calibrate its parameters. Technically the calibration was done on an amended dataset in which each household/workplace represented in the demand function chooses a location based on the artificial choice-set. It means that if a household/workplace select the first district as its new location (regardless of the previous one), it also means that all other alternative locations are rejected. Based on these choices coefficients can be estimated for the independent variables and for the utility correction factor.

Finally, the population model was also calibrated for the annual changes of the size of the given age groups, the number of births and deaths.

Due to the aforementioned calibration issues, compared to the original LUTI model there were a few changes:

- walking as a transport mode is neglected;
- trip distribution and mode choice is modelled separately;
- greenfield and brownfield developments within the real-estate market module are not differentiated due to a lack of data;
- there is an external variable for the labour market module as conventional changes of the explanatory variables have not described the phenomena well enough (meanwhile the variable of available floorspace is not included in the model as it happened to be insignificant);
- households are not differentiated based on income as there was not reliable data on actual income of residents;
- there is an extra variable for institutional environment within the housing market module which adds to the explanatory power of the model;
- motorization became an external variable as available data (GDP, fuel prices, travel times, accessibility, etc.), as it was not enough to give an adequate prediction.

#### **4. Results**

Table 2 shows the calibration dimension and the goodness of fit for each module. It is important to note that in this chapter modelled values are compared to observed values which mean that the values of the saturated model would equal to the observed ones ( $y=x$ ). Observed values are really observed in terms of land-use data (e.g. the changes of the number of households), while these are original values in case of the transport-related values (e.g. the cell values of the direct demand matrices of the official transport model for Budapest).

Land-use and demographic modules provided a quite good fit to actual data. Transport-related modules are worse in that sense, but one should take into consideration that these modules are mostly consecutive and small errors in the first module (trip generation) might be multiplied in latter stages. However, coefficient values of determination calculated for the cells of the matrices suggest that these matrices should not be applied directly in the transport model. Pivoting the changes of these synthetic matrices to the direct ones can bridge the gap and still provide reliable modelling results. It is also important to take into consideration that it was not intended in this research to replicate the more comprehensive and detailed official transport model of Budapest. The purpose was to provide a less detailed, but still reliable transport modelling background in order to be able to carry out the calibration of the land-use modules. Fig. 3 illustrates the differences between the travel time distributions of the model and the official one, while Figure 4, 5, 6 and 7 show the differences between the modelled and observed changes of the number of new housing units, households, workplaces in service and production sector respectively. All of these differences can be considered acceptable and hint that the model works reliably.

Table 2: Results of the model calibration

Module	Calibration		Calculated R <sup>2</sup> : (SST-SSE) /SST	Comment	
	spatial dimension	time dimension			
Trip generation	192 zones (sub-district level: 162+30 suburban)	2014	0.93	R <sup>2</sup> is calculated for the production	
Trip distribution			0.80	R <sup>2</sup> is calculated for the cells of the matrices	
Mode-choice			Private car		0.51
			Public transport		0.63
Bicycle			0.22		
Freight modelling				0.18	
Rent and land price	28 zones (districts level: 23+5 suburban)	2007-2013 per annum	0.98		
Real-estate market		2007-2013 as a whole	0.71	The suburban areas are not included in the module	
Housing market			0.87		
Labour market			Services	0.82	
			Production	0.77	
Population	-	2007-2013 per annum	0.99		

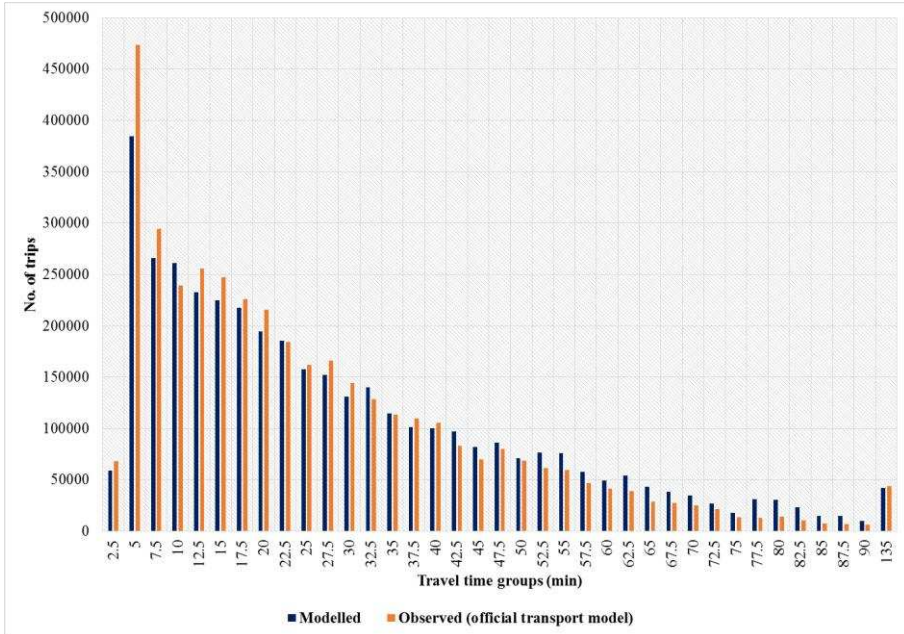


Figure 3: Travel time distributions of the LUTI model and the official transport model for Budapest

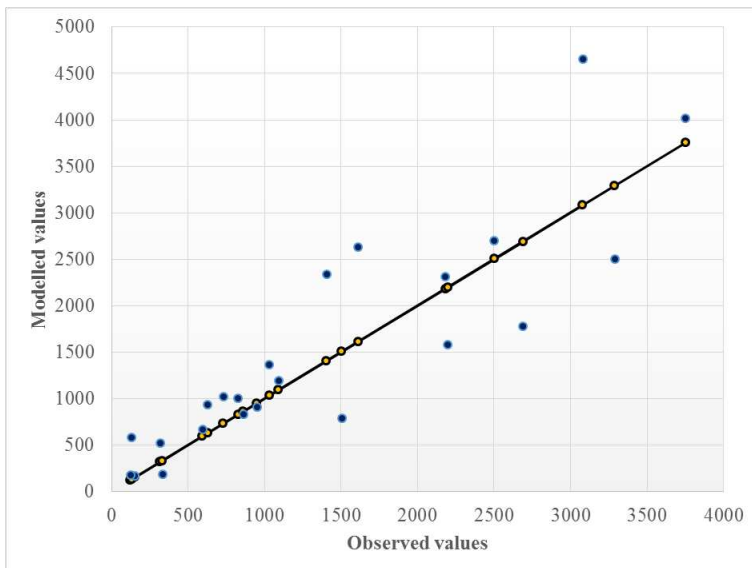


Figure 4: Differences between modelled and observed changes of the number of new housing units

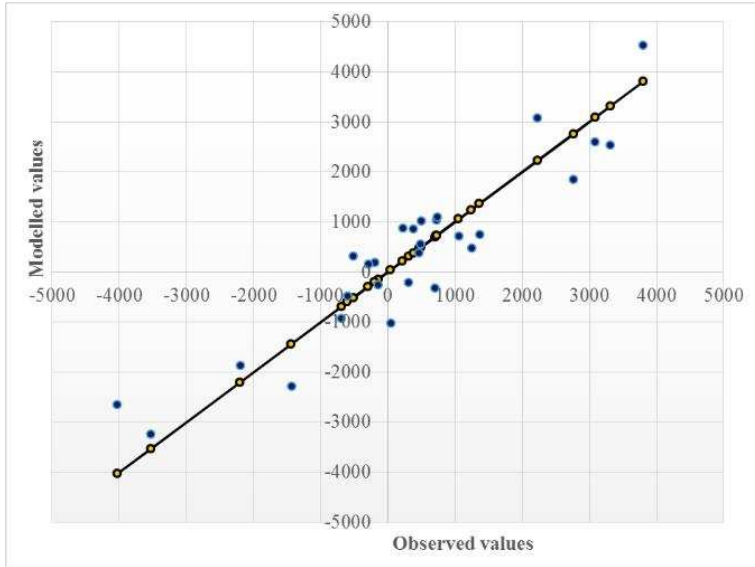


Figure 5: Differences between modelled and observed changes of the number of households

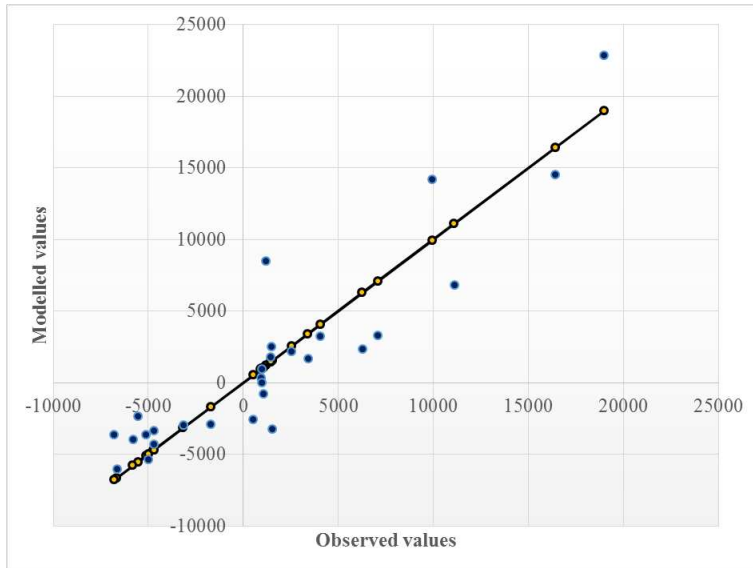


Figure 6: Differences between modelled and observed changes of the number of workplaces in service sector

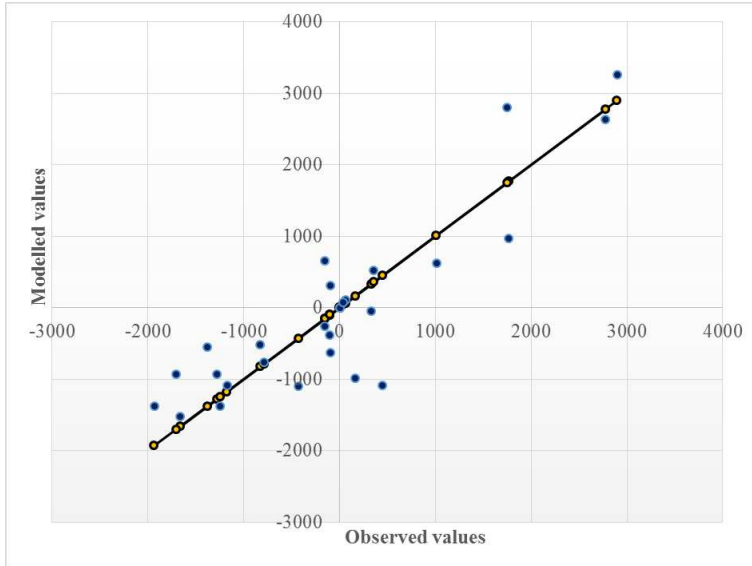


Figure 7: Differences between modelled and observed changes of the number of workplaces in production sector

Table 3, 4 and 5 show the calibrated values of model coefficient and parameters. It is encouraging that the coefficients of the land-use modules were of the correct (theoretically expected) sign and significant at the 85-95% level. This chapter is focusing on the interpretation of these results.

Table 3: Calibrated model parameters and coefficients

Module	a	b	c	d	e	f
Trip generation	NWR trip component (calculated)	workers going to work	students going to school	workers returning-home rate	students returning-home rate	
	0.243	0.8	0.4	0.71	0.8	
Mode-choice	constant	travel time	parking time	road charges	vehicle operating cost	
Private car	0	-0.18	-0.36	-0.25	-0.03	
Public transport	constant	in-vehicle time	transfer time	origin waiting time	fare	
	-3.25	-0.18	-0.36	-0.27	-0.18	
Bicycle	constant	travel time				
WR	-4.3	-1.08				
NWR	-3.4	-0.85				
Inter-mediate calculations	Access-ibility scaling	RT-DF scaling	RT-DF elasticity	LP-DF scaling	LP-DF elasticity	
	-1	-0.038	-0.112	-0.003	-0.509	

Real-estate market	UncDB scaling	UncDB elasticity	ConstDB scaling	ConstDB elasticity		
	50	1.6	0.000025	1.6		
Housing market	Accessibility (normalized min)	Housing quality	Green spaces	Institutional environment	Rent rate (for a month)	Utility corr. factor
	0.015	0.169	0.382	0.101	-0.125	0,775
Labour market	Accessibility (normalized min)	Cost of building	Utility corr. factor			
Services	0.032	-0.057	1.22			
Production	0.040	-0.024	1.25			
Population	Pot. → 0-15	0-15 → 16-65	0-15 → D	16-65 → 65+	16-65 → D	65+ → D
	0.072	0.0715	0.001	0.0166	0.005	0.054

Table 4: Calibrated parameters for the trip distribution model (for travel time bins)

k	1	2	3	4	5	6	7	8
Travel time range	10-	10-20	20-30	30-40	40-50	50-60	60-75	75+
$\beta_k$	0.04	0.07	0.065	0.06	0.055	0.05	0.045	0.035

Table 5: Other parameters of the model

Other parameters	Value
Travel time budget	58 mins
Average household size	67 m <sup>2</sup>
Average workplace size	12 m <sup>2</sup>
Average time-span for living in the same place	25 years
Average life-span for businesses	20 years
Value of time (work-related)	0.1 EUR/min
Value of time (non-work-related)	0.07 EUR/min
Average building cost	530 EUR/m <sup>2</sup>

At first, the real-estate market module was able to predict the overall demand for building new housing units and the average zonal profitability seemed to be a good indicator for the location choice of the development. The estimated parameters are much more different than those of the DELTA model from where the method is originated, but the Hungarian construction sector is also different (both in its scale and also in terms of the elasticity to profitability) from the British.

In the housing market module the explanatory variables combined with the correction factor for size described the changes in the number of households quite well. Fig. 8 shows the deviation of calculated utility for each district from the average utility (which is the basis of the applied multinomial logit model) compared to the actual changes in the households.

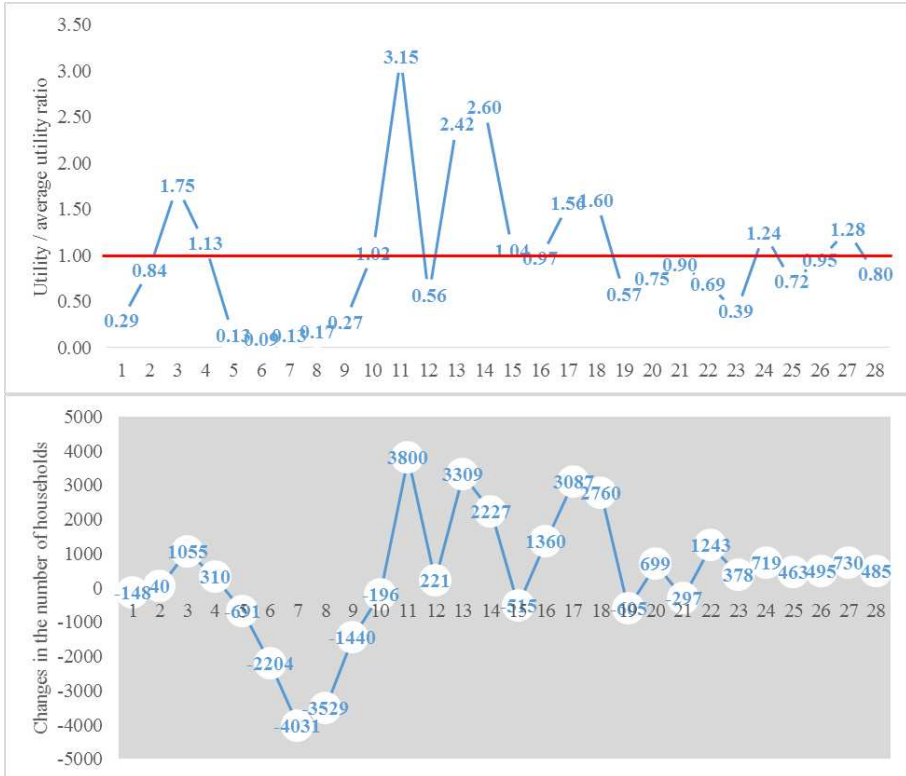


Figure 8: Deviation of the calculated utility from the average utility for each district (top) compared to the actual changes in the number of households (bottom)

According to Table 3, the coefficient of accessibility is around 0.015. The variable of accessibility describes a normalized weighted value (in minutes) for every potential trip purposes. The magnitude of the coefficient is in line with values from other researches in the UK (0.01-0.07 mins/trip, [17]). It is also reassuring that if value of time (VOT) is derived from the coefficients (i.e. the ratio of the accessibility coefficient to that on rent) it is also somewhere of the expected magnitude. As rent rate is calculated for a month, accessibility coefficient needs an adjustment with the average monthly trips rate (division by the estimated value of 45). The mentioned ratio of utility per minute to utility per money implies a VOT of about 0.16 EUR/hour. This is quite low compared with the value used in the transport model (4.2 and 6 EUR/hour for non-work-related and work-related trips respectively). A potential explanation for the difference could be the way in which accessibility and rent rates are measured. In addition to that there are also differences in the way of how accessibility is built into the housing market module to how travel time is perceived in travel choices in which standard values of time are estimated. Very similar results were found by [17] on the same issue. It also seems to be logical that VOT in a location choice aspect could be lower than in a transport sense.

In the labour market module only the variables of accessibility and cost of building have been found to be significant. Other variables previously suggested by other models

(e.g. the available floorspace from the MARS model) were not included for this reason. An external variable was also calibrated with the intention to control areas with different characteristics which seemed to be relevant for business location choice. The values of these external factors are shown in Fig. 9.

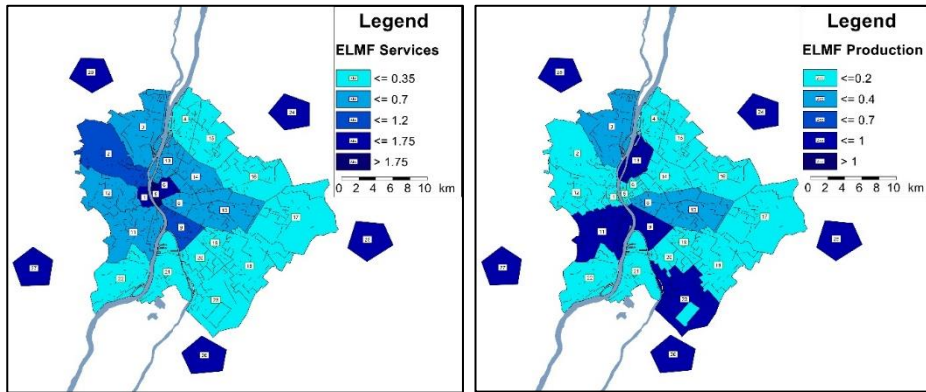


Figure 9: Values of the external utility factors in the labour market module for services (left) and production sector (right)

In terms of the other, complementary parameters there are also some interesting results. First of all the travel time budget calculated from the base year (2014) model is around 58 mins/day. This is slightly lower than those international values reported by Schafer and Victor [18] (spread from 60 to 80) and values for Budapest by Fleischer and Tir [19] (around 75). An obvious explanation can be that walking as a transport mode is not included. In addition to this, suburban areas are also not fully covered. Within the model only those residents are included who make a trip to or through Budapest. The number of these residents is also taken into consideration in the calculation of the travel time budget. However, those trips are excluded that these people have towards other destinations which are not affect the capital city. The mentioned two factors can reduce the travel time budget by around 20-25%. Secondly, the values of average time-span of living in the same place (ATSL) and life-span of businesses (ALSB) were also calibrated. There was not any official or strongly reliable data on these values, however, during the calibration 25 and 20 years were found to be fit to the observed changes. It provides some background to ATSL that according to some national statistics on the housing market an average resident moves 3.4 times during a lifetime [20], which implies a value around 22-25 years. In terms of ALSB the only relevant data based on private business information systems (Opten statistics) that the fluctuation is nearly 50% among companies in every 5 years. That would imply a value below 10 years. However, the ALSB value is much more complicated and it is also common that there is a fluctuation in terms of companies but the workplace and its location remains in its previous state.

Table 6 provides some details on the coefficients of the land-use modules. All of the variables found to be significant at the 95% level apart from the rent rate in the housing module which is significant at the 85% level.

Table 6: Details of the calibration results for the land-use modules

Explanatory variable	Coefficient	Exp(Coeff.)	Standard Error	Significance
Housing market module				
Accessibility	0.015	1.015	0.007	0.045
Housing quality	0.382	1.466	0.061	~ 0.0
Green spaces	0.169	1.184	0.037	~ 0.0
Institutional environment	0.101	1.106	0.049	0.038
Rent	-0.125	0.883	0.081	0.121
Utility corr. (size)	0.775	2.171	0.124	~ 0.0
Labour market module - Services				
Accessibility	0.032	1.033	0.006	~ 0.0
Cost of building	-0.057	0.944	0.014	~ 0.0
Utility corr. (size)	1.22	3.387	0.075	~ 0.0
Labour market module - Production				
Accessibility	0.040	1.040	0.04	~ 0.0
Cost of building	-0.024	0.976	0.12	0.008
Utility corr. (size)	1.25	3.490	0.068	~ 0.0

Finally, a test running of the model has been carried out in order to demonstrate what LUTI modelling can bring in terms of differences in traffic volumes. Starting from 2007 as a base year the whole model run until 2013 and predicted the changes in the land-use and transport system annually. Another scenario was to give a prediction from 2007 up until 2013 without any change in the land-use system (that is what traditional transport modelling does). Then these modelling results were compared to that of the actual model for 2013 (used as a reference). Fig. 10 shows the differences in private (left side) and public transport (right side). On the top is the difference between the actual 2013 model and the model for 2013 derived from 2007 with the full LUTI model, while in the bottom it is the difference between the actual 2013 model and the model for 2013 derived from 2007 without land-use changes.

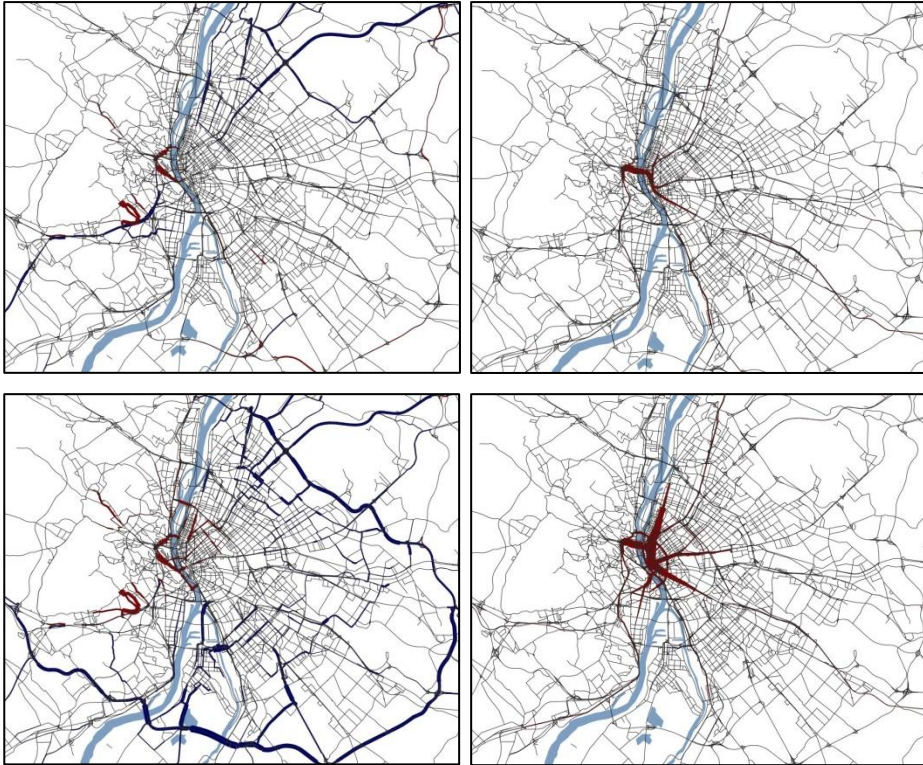


Figure 10: Differences in private (left side) and public transport (right side) traffic volumes between “model 2013” and the model for 2013 derived from 2007 with the full LUTI model (top), plus between “model 2013” and the model for 2013 derived from 2007 without land-use changes (bottom)

## 5. Conclusions

Based on the results of this paper it is undeniable that excluding land-use effects of transport in modelling such schemes could cause a serious distortion even in a shorter time period (e.g. in 7 years). It is not the quantifiable indicators (total travel time, total distance covered or vehicle operating cost) that can have a considerable change, but the spatial differences can be significant, especially if the impacts of a certain project are under estimation. It seems that such land-use effects and feedbacks can no longer be disregarded as it is not in accordance with the desire of improving transport modelling practice. Moreover, it makes no sense to constantly develop better and better transport models or modelling parts (e.g. traffic assignment methods) while the gain with the improvement is far less than losses coming from neglecting land-use effect. From this point of view, an ideal solution might be to establish a modelling framework which takes into account every important aspect and then improve its parts in a way which ensures a sustained integrity. Otherwise there is an imminent risk that isolated best-practices are to be created which could be hardly integrated with each other.

This paper suggests that land-use effects can be included and semi-sophisticated (but still reliable) LUTI models could be created even if available data are narrow. This approach is also practical and can overcome general obstacles of time, cost and data availability issues. Besides if such a LUTI model is created and constantly used it can be a platform of further development and may also influence data collection which can aid further model development going forward.

Ultimately, further steps of this research are drafted. The next step should be to carry out case studies (tests) for the estimation of real transport investments (to see whether the model performs as expected) and compare the results with conventional and international ones. For the city of Budapest these case studies could be a following: impact of the recently implemented metro line M4, the planned traffic calming of the city centre (which may include congestion charging) and a scenario for a rapid fuel price increase.

## References

- [1] Hamilton-Baillie B: Shared space: reconciling people, places and traffic. *Built Environment*, Vol. 2, pp. 161–181, 2008.
- [2] Bonsall P: Legislating for modal shift: background to the UK’s new transport act. *Transport Policy*, Vol. 7, pp. 179–184, 2000.
- [3] Kjemtrup K, Herrstedt L: Speed management and traffic calming in urban areas in Europe, a historical view. *Accident Analysis and Prevention*, Vol. 1, pp. 57–65, 1992.
- [4] Horváth B: Rendszerszemléletű stratégiai tervezés. In: Hamarné Szabó Mária (ed.): *Közlekedésfejlesztés Magyarországon*, Palatia Kiadó, Budapest, 2016. 228 p.
- [5] Gaál B: Status of Land Use and Transport modeling in Hungary. In: Esztergár-Kiss Domokos, Válóczy Dénes, Tóth János, Varga István (ed.): *4th International Conference on Models and Technologies for Intelligent Transportation Systems (MT-ITS)*, BME Közlekedésmérnöki és Járműmérnöki Kar, Budapest, 2015. 536 p.
- [6] Juhász M: Development of a land-use and transport interaction model as a part of a policy assessment framework for urban traffic calming. *Pollack Periodica*, Vol. 10, pp. 81–92, 2015.
- [7] Doi K, Kii M: Looking at sustainable urban mobility through a cross-assessment model within the framework of land-use and transport interaction. *International Association of Traffic and Safety Sciences Research*, Vol. 35, pp. 62–70, 2012.
- [8] Bravo M, Briceño L, Cominetti R, Cortés CE, Martínez F: An integrated behavioral model of the land-use and transport systems with network congestion and location externalities. *Transportation Research Part B*, Vol. 44, pp. 584–596, 2010.
- [9] Still BG., May AD., Bristow AL: The assessment of transport impacts on land use: practical uses in strategic planning. *Transport Policy*, Vol. 6, pp. 83–98, 1999.
- [10] Simmonds D, Georgieva S, Simpson T, Fotheringham A: Recent Developments in ULTrA: Unified Land-use and Transport Appraisal. *Proceedings of the European Transport Conference 2015*. AET, Frankfurt. 2015. Paper id: 4766.
- [11] Simmonds D, Still BG: The implementation of the DELTA/START land use transport model, Working Paper 494, ITS University of Leeds, Leeds. 1997.

- [12] Pfaffenbichler P: The strategic, dynamic and integrated urban land use and transport model MARS (Metropolitan Activity Relocation Simulator). Doctoral Thesis, Fakultät für Bauingenieurwesen der Technischen Universität Wien, Wien. 2003.
- [13] Zondag B, de Jong G: The development of the TIGRIS XL model: A bottom-up approach to transport, land-use and the economy. *Research in Transportation Economics*, Vol. 31, pp. 55–62, 2011.
- [14] Dobson A, Richmond E, Simmonds D: Design and use of the new Greater Manchester Landuse/Transport Interaction Model (GMSPM2). *Proceedings of the European Transport Conference 2009*. AET, Noordwijkerhout. 2009. Paper id: 3224.
- [15] Ortúzar JD, Willumsen LG: *Modelling Transport*, 4th Edition. Wiley, Chichester. 2011. p. 586.
- [16] Modell Tercett Konzorcium (Fómterv Plc. – Közlekedés Ltd. – Trenecon Ltd.): *Egységes Forgalmi Modell (EFM) Budapest és Agglomerációjának teljes területére – Modellezési és használati útmutató*. BKK, Budapest. 2015. p. 276.
- [17] Reville E, Simmonds D: Calibrating a household relocation model for Leicestershire. *Proceedings of the European Transport Conference 2011*. AET, Glasgow. 2011. Paper id: 3756.
- [18] Schafer A, Victor DG: The future mobility of the world population. *Transportation Research Part A*, Vol. 34, pp. 171-205, 2000.
- [19] Fleischer T, Tir M: The transport in our time-budget. *Regional Statistics*, Vol 6, No 2, pp. 54–94, 2016.
- [20] Hungarian Central Statistical Office: *Miben élünk? A 2015. évi lakásfelmérés főbb eredményei*. KSH, Budapest. 2016. p. 52.

# Rotational Motion Modelling for Numerical Analysis of Electric Machines

D. Marcsa<sup>1,2</sup>

<sup>1</sup>**Knorr-Bremse Commercial Vehicles, Research and Development Institute,  
Engineering Calculation  
Major u. 69., 1119, Budapest, Hungary  
E-mail: daniel.marcsa@knorr-bremse.com**

<sup>2</sup>**Széchenyi István University, Department of Automation  
Egyetem tér 1., 9026, Győr, Hungary**

**Abstract:** The paper presents a brief review of the movement modelling methods of electric machines and the two most common used torque calculation techniques. After the classification of single-layer moving band methods, a low computation cost and an easily realisable new variant of this movement modelling technique is proposed. To study the accuracy of proposed moving band technique equipped with Arkkio's method and Maxwell's stress tensor method for torque calculation an international benchmark problem used. Further, to check the applicability, the proposed method has been used to analyse a three-phase switched reluctance motor. The results of proposed method have been compared to analytical and numerical results.

**Keywords:** *Rotational motion modelling, Finite element method, Torque calculation, Electric machine*

## 1. Introduction

The numerical design and simulation of electromechanical actuators, and within that rotating electric machines are one of the main focus points of many researchers and research groups nowadays due to the hybrid and electric vehicles [1–4]. The aim of a numerical field calculation is to explore the overall behaviour of the analysing device, including all possible physical side effects simultaneously. To understand the behaviour of electric machines and to be able to intensify it, the accurate knowledge of the parameters governing physical effects must be known. The so-called coupled problem can distinguish between the single effects and may help to better understand the effects and their mode of operation [5–7].

A variety of numerical methods exists, but the most popular technique is finite element method (FEM) [8–10] among researchers in low-frequency electromagnetic applications. The mathematical description of the electromagnetic field can be derived from Maxwell's equations with appropriate boundary and interface conditions [8, 11]. However, Maxwell's equations based formulations itself is only enough to time independent or steady-state simulations of rotating machines, it is not suitable for dynamic analysis.

The coupling plays an important role in the dynamic analysis of machine performance. The acceleration and mechanical transient of driving electric motor, so the propulsion performance is significant properties in the automotive industry. Consequently, it is important to take into consideration rotor movement in simulation via coupling [10–12]. There are many possibilities for stator-rotor connection and movement modelling, but most of them are computationally intensive or the implementation is difficult.

This article describes a brief stagger around the field of movement modelling in finite element method for electric machines. Moreover, I propose a simple and computationally efficient technique for modelling the rotational motion of the rotor. The torque calculation is also an important part of the dynamic simulation, therefore the paper briefly reviews the two most widely used methods. The applicability and performance of the proposed technique are analysed using an international benchmark problem and a three-phase switched reluctance motor. The combinations of presented torque calculation methods with movement modelling methods are also analysed via the simulation results.

## 2. Rotational Motion Modelling Methods

In this paper, the stator (fixed part) – rotor (mobile part) coupling classifies to the nature of the geometrical decomposition of the machine model. The field equation is applied to both parts, and the relative motion is taken into account in the air-gap, an ideal place to do it since it is non-ferromagnetic, non-conductive and without source. Based on it, one can distinguish between *air-gap interface* and *sliding surface* methods [10, 12].

### 2.1. Methods with Air-Gap Interface

In methods of the air-gap interface, the air-gap or a part of it is considered as a separate domain with interfaces both to fixed and mobile part. The popularity of methods' group well shows the variants of air-gap discretisation technique as the macro-element method [10, 13], the moving band [10, 14, 15, 17, 18], the boundary integral method [19] and the discontinuous Galerkin technique [20]. In the following, the macros-element and moving band method will be reviewed briefly.

First, the so-called *macro-* or *air-gap element* technique [10, 12, 13] used to create the continuity between interfaces of stator and rotor meshed domains with an unmeshed air-gap region. This method is used analytical solution of  $\nabla \times (\nabla \times \vec{A}) = \vec{0}$  equation in

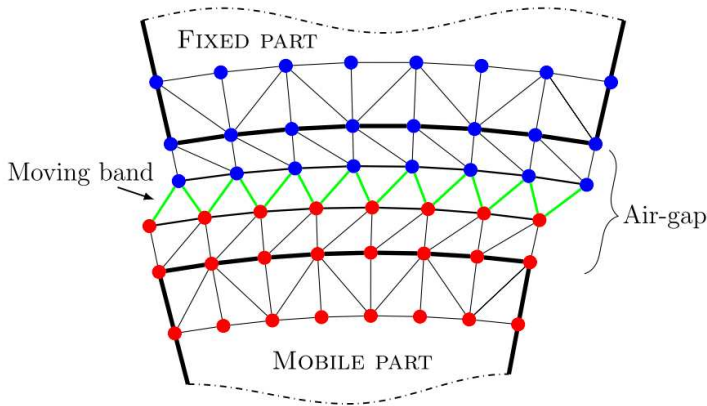


Figure 1. Single-layer moving band with triangular discretisation.

polar coordinate system which takes into account rotation of mobile part. The analytical solution is based on a truncated Fourier-series expansion of the  $\vec{A}$  magnetic vector potential, where 100 to 200 harmonic terms give good accuracy [10]. Together with a high harmonic number, this technique introduces a dense part in the sparse finite element system of the equation which is also a drawback. An advantage of the air-gap element technique is that the results can be very accurate because of the high order of the field representation in the air-gap region.

However, to avoid the dense matrix block, and to use the long standing FEM solvers, proposed the *moving band method* (MB) [10, 14–16] which is much more popular technique nowadays. In this method, the coupling between interfaces is commonly made by finite element placed in the air-gap, as it can be seen in Fig. 1. The simplest version of it, when each time step re-mesh the air-gap, however, this is not so computationally efficient. A more sophisticated way is to change the connectivity matrix between fixed and mobile part, while considered the element distortion.

## 2.2. Methods with Sliding-Surface

In *sliding-surface techniques* (SS), the rotational movement of the rotor is modelled at a common interface somewhere in the air-gap. The simplest variant of this group is the *locked-step approach* [21], where equidistant discretisation is applied, and the rotor rotates with an integer number of an angle between two adjacent nodes in each step. This is the conform version of sliding surface when the stator and rotor nodes are connected in each step, so the continuity maintains between the fixed and mobile parts. It is suitable for analysing the steady state of the machine but too severe for technical machine models. The dynamic modelling with the locked-step approach is computationally intensive because

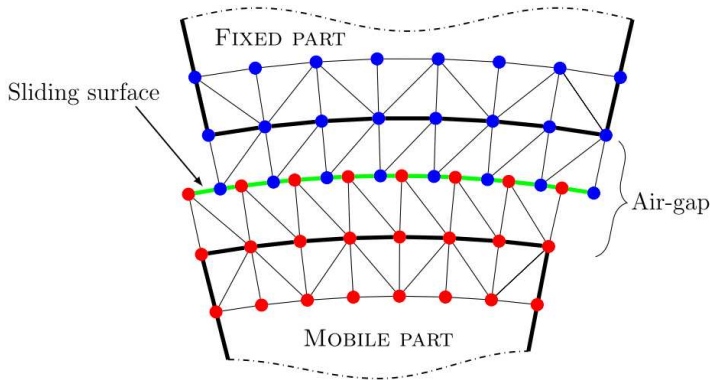


Figure 2. Sliding surface with nonconform mesh.

every time steps varies the length of time steps, namely the system matrix.

In general, the sliding surface techniques allow non-matching grids as you can see in Fig. 2. Therefore ensure the continuity of vector potential across the sliding surface an addition constraint. The most common techniques which are applied to enforce the continuity the polynomial (first or second order) interpolation [22], trigonometric interpolation [18, 23], Lagrange-multipliers [24, 25] and mortar projection [26, 27]. The common in all methods is one of the parts is the slave and the other one is the master surface, and the unknown variables of slave surface are described by master surface variables.

### 2.3. Single-Layer Moving Band

Based on the literature, the single-layer moving band (later moving band) is a widely used technique, but only in [10, 14, 16, 17] are mentioned or described the implementation of it. According to the descriptions, the following three types can be distinguished.

- (1) **Basic moving band** [14]: This variant is the origin of the technique. This version is not dealing with the distortion of finite elements in the moving band. The operation of the technique, when the displacement is larger than the angle between two adjacent elements, than modified the connectivity matrix of moving band elements.
- (2) **Moving band with quadrilateral mesh** [10, 16]: In this case, quadrilateral finite elements are used in the band, which are divided four triangular elements by the diagonals. The usage of triangles depends on the quality of elements and the angular displacement. To determine the quality of elements using a special formula which is based on the length of edges.

(3) **Moving band with trigonometric interpolation** [17]: In this case, contrast to previous methods, the appropriate elements of system matrix will vary depending on the displacement. The number of finite elements decreases because of the use of trigonometric interpolation, however, the solution of the equation system is needed an iterative solver which incorporating Fast Fourier Transformation [18].

### 2.3.1. Proposed Method

The discretisation of proposed single-layer moving band boundaries in 2-D is equidistant with the same node and edge number. In this case also the connectivity matrix modified as variants (1) and (2). The base of this technique also the quadrilateral element as in (2), which is divided into two triangles depends on the  $\alpha$  angle, as a measure of the distortion.

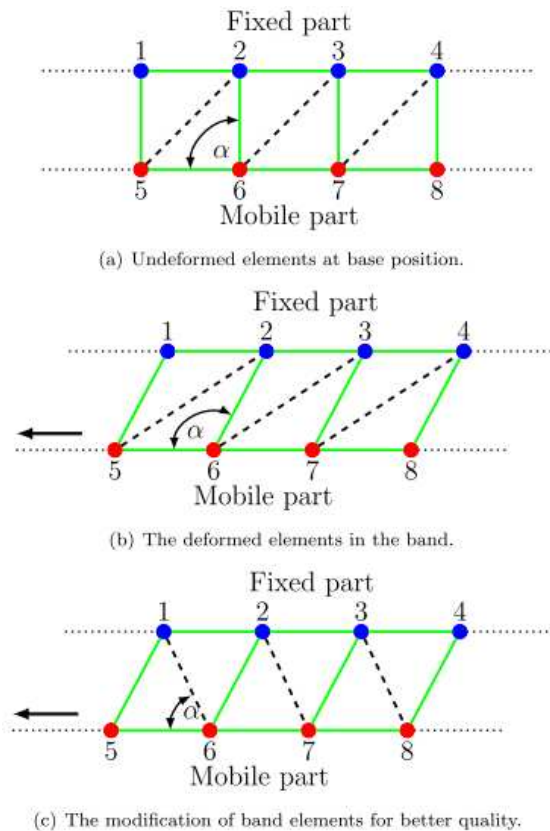


Figure 3. Proposed single-layer moving band method.

This can be seen in Fig. 3. To determine all band elements quality is enough to examine only one element by the following equation

$$\text{Quality factor} = \begin{cases} \text{good} : & \text{if } \alpha \leq 90^\circ \\ \text{bad} : & \text{if } \alpha > 90^\circ \end{cases}, \quad (1)$$

because all elements have the same shape.

The proposed method takes into account the element distortion, unlike the (1) version. The computation cost of elements quality is less in this case than in (2). Further, the implementation of it is much easier than the (3), and does not require special solver. The accuracy of the proposed method is not so high with the coarse mesh, however the usage of dense finite element mesh required for accurate torque calculation in the air-gap region, so the accuracy of this technique appropriate. This is supported by the used examples.

### 3. Torque Calculation Methods

The torque calculation also a cornerstone of rotational motion modelling as the before mentioned methods. In the followings, the two most common used torque calculation methods, Maxwell's stress tensor method (MST) [11, 16, 25, 28] and method proposed by Arkkio (AM) [28, 29] are briefly reviewed.

#### 3.1. Maxwell's stress tensor method

The electromagnetic torque acting on the rotor of an electric machine may be calculated by integrating the Maxwell's stress tensor  $d\vec{F}$  along a line  $\Gamma$  placing in the air-gap in two-dimensional case:

$$\vec{T}_e = l \int_{\Gamma} (\vec{r} \times d\vec{F}) \, d\Gamma = l \int_{\Gamma} \left( \vec{r} \times \left[ \mu_0 (\vec{H} \cdot \vec{n}) \vec{H} - \frac{\mu_0}{2} H^2 \vec{n} \right] \right) d\Gamma, \quad (2)$$

where  $l$  is a depth of the domain in the  $z$ -direction,  $\vec{r}$  is the position vector linking the rotating axis to the elements  $d\Gamma$ ,  $\Gamma$  is a surface, which is placed around the air-gap,  $\mu_0$  is the air magnetic permeability,  $\vec{H}$  is the magnetic field strength,  $H = |\vec{H}|$  is the absolute value of the magnetic field strength and  $\vec{n}$  is the normal unit vector to the surface.

#### 3.2. The Method Proposed by Arkkio

This method is a variant of the Maxwell's stress tensor method and consists in integrating the torque given by equation (2) in the whole surface (in 2-D) of the air-gap comprises between the radii  $r_R$  and  $r_S$ . The torque is computed with the following equation:

$$T_e = \frac{l}{\mu_0 (r_S - r_R)} \int_S r B_r B_\theta \, dS, \quad (3)$$

where  $S$  is the region between the radii  $r_R$  and  $r_S$ .  $B_r$  and  $B_\theta$  are the radial and tangential component of magnetic flux density,  $r$  is the distance between the origin and the midpoint of the integration segment.

## 4. Examples

To check the validity of presented and proposed methods, an international benchmark problem of COMPUMAG Society, the T.E.A.M. 30a three-phase induction motor [11, 30] has been solved and compared the known analytic solution. This test problem used to analyse the combination of torque calculation methods with moving band and sliding surface technique. Further, to present the applicability of proposed method, here a three-phase (6 stator and 4 rotor poles) switched reluctance motor [31] (SRM) has been solved and compared the simulation results.

### 4.1. Problem T.E.A.M. 30a - Induction Motor

As a test problem, a 2-D eddy current field analysis of three-phase test induction motor used. The detailed description of it including geometry and material parameters and the analytic solution can be found in [30]. A numerical solution of this problem a small above the synchronous speed can be seen in Fig. 4. This figure shows the magnetic vector potential distribution and the equipotential lines into the machine.

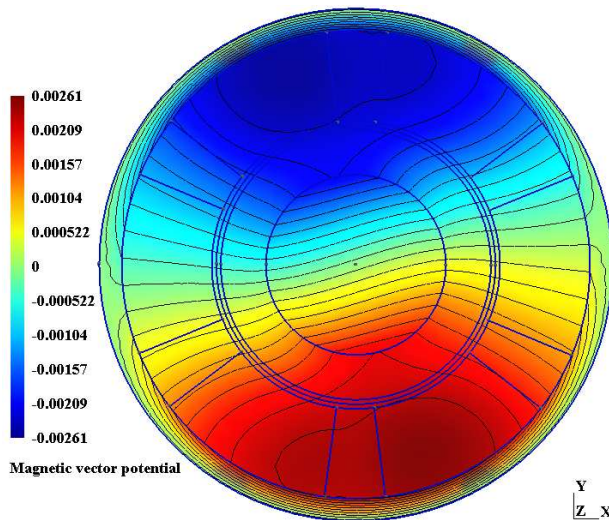


*Figure 4. Field distribution in the T.E.A.M. 30a three-phase test motor at 400 rad/s.*

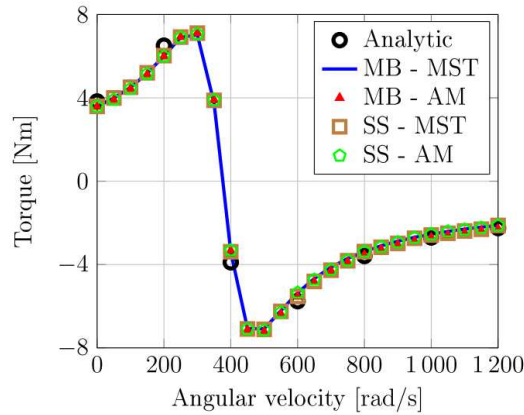


Figure 5. Calculated torque - angular velocity curves.

Fig. 5 shows the results of torque calculation. The analytic solution is given with 200 rad/s step within the range of analysis (0, . . . , 1200 rad/s), wherein the numerical results are plotted with 50 rad/s step. The calculated numerical results show good agreement with the given analytic calculation. The biggest difference between analytic and numerical results is at 400 rad/s. The reason for this big difference is the closure of synchronous speed ( $\approx 377$  rad/s), where the torque–speed curve of the induction machine is steep. A small speed difference leads significant torque difference in this speed range.

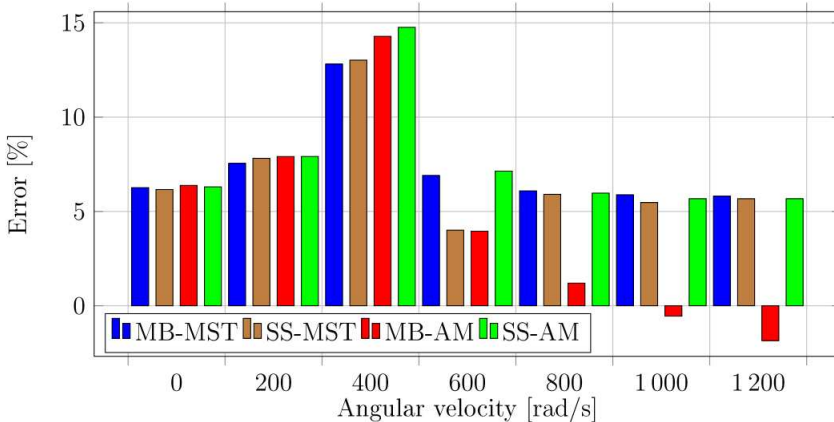


Figure 6. Bar plot of torque calculation error.

The above statements also supported by the next figure, Fig. 6, where the torque calculation errors are summarised in a bar plot. The results of combined methods are approximately same, except the moving band with Arkkio’s method above 600 rad/s angular velocity. Based on the results, the proposed moving band with Arkkio’s method and sliding surface with Maxwell’s stress tensor method have the best torque calculation performance, which agree with the literature [16, 25, 28].

#### 4.2. Switched Reluctance Motor

After the benchmarking, a 6 stator pole and 4 rotor pole switched reluctance motor has been analysed by FEM. The geometry and material parameters of this application example are from examples of Agros2D free finite element software [31]. Fig 7 shows the shape and results of the three-phase switched reluctance motor after the switching instance of winding excitation. The figure shows the absolute value of magnetic flux density distribution and equipotential lines.

Fig. 8 shows the calculated results, the torque in the function of mechanical angle. In this case, only the results of two combinations, the proposed moving band with AM and sliding surface with MST are analysed. The sliding surface results are used as the validation of implemented finite element code. The solution of Agros2D is the reference solution, which is based on the co-energy variation torque calculation method [10, 28] with adaptive

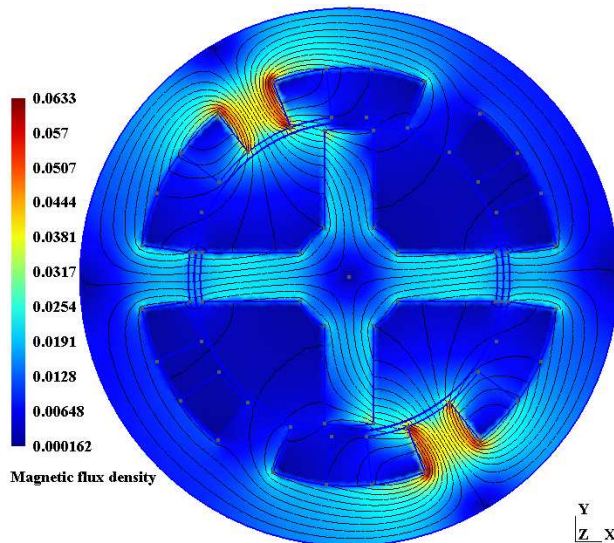


Figure 7. Field distribution in 6/4 switched reluctance motor.

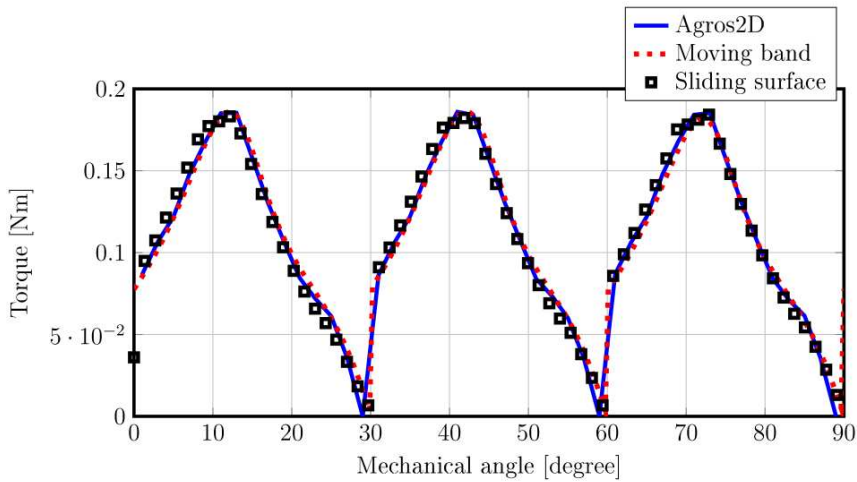


Figure 8. Torque curves in the function of mechanical angle of rotor.

mesh refinement technique. The results of presented methods show good agreement with the calculated torque from Agros2D, but the result with proposed method shows better relation.

## 5. Conclusion and Future Works

The paper has discussed rotational motion modelling and two most common used torque calculation techniques of electric machines. The available single-layer moving band methods have been classified based on the implementation and proposed a low computation cost and an easily realisable new variant of movement modelling technique. The accuracy and applicability of proposed single-layer moving band method are checked via two rotating machine examples.

It can be concluded that the accuracy of the proposed method is appropriate for electric machine modelling and almost the same than the sliding surface method. These conclusions also supported by simulated results, where the comparisons show good agreement.

The aim of the further research is to find a way to solve three-dimensional multiphysics problems including motional voltage-fed eddy-current field problems with the proposed movement modelling technique.

## References

- [1] Sarigiannidis, A. G., Beniakar M. E., Kladas A. G.: *Hybrid Analytical-FEM Methodology for Loss Evaluation in Traction Motors for Electric Vehicle Applications*, in 2016 IEEE Conference on Electromagnetic Field Computation (CEFC), Miami, pp. 1–4, 2016  
DOI: 10.1109/CEFC.2016.7816130
- [2] Kim C. K.: *A Novel Calculation Method on the Current Information of Vector Inverter for Interior Permanent Magnet Synchronous Motor for Electric Vehicle*, IEEE Transactions on Magnetics, Vol. 50, No. 2, pp. 829–832, 2014  
DOI: 10.1109/TMAG.2013.2279555
- [3] Xiping, L., Ya, L., Zhangqi, L., Tao, L., Zhenhua, L.: *Analysis and design of a high power density permanent magnet-assisted synchronous reluctance machine with low-cost ferrite magnets for EVs/HEVs*, COMPEL - The international journal for computation and mathematics in electrical and electronic engineering, Vol. 35, No. 6, pp. 1949–1964, 2016  
DOI: 10.1108/COMPEL-05-2016-0233
- [4] Haiwei, C., Bo, G., Longya, X., Woongchul, C.: *Optimal design of synchronous reluctance machine: A feasible solution to eliminating rare earth permanent magnets for vehicle traction applications*, COMPEL - The international journal for computation and mathematics in electrical and electronic engineering, Vol. 33, No. 5, pp. 1569–1586, 2014  
DOI: 10.1108/COMPEL-09-2013-0287
- [5] Roger, D.: *Electrical Machines ... a Challenge for the Year 00 ?*, International Compumag Society Newsletter, Vol. 12, No. 1, pp. 5–7, 1999
- [6] Kawase, Y.: *Magnetic Field Analysis Coupled with Electric Circuit and Motion Equation*, International Compumag Society Newsletter, Vol. 7, No. 3, pp. 12–16, 2000
- [7] Preston, T. W.: *Implementation of the Finite Element Method into an Industrial Design Environment*, International Compumag Society Newsletter, Vol. 8, No. 3, pp. 2–8, 2001
- [8] Kuczmann, M., Iványi, A.: *The Finite Element Method in Magnetics*, Akadémiai Kiadó, Budapest, 2008
- [9] Luomi, J.: *Finite Element Methods for Electrical Machines*, Chalmers University of Technology, Gothenburg, 1993
- [10] Bastos, J. P. A., Sadowski, N.: *Electromagnetic Modeling by Finite Element Methods*, Marcel Dekker, New York, 2003

- [11] Marcsa, D.: *Finite Element Analysis of a Solid-Rotor Induction Machine*, Acta Technica Jaurinensis, Vol. 3, No. 2, pp. 61—70, 2010
- [12] De Gersem, H., Weiland, T.: *Reformulation and Generalisation of the Air-Gap Element*, International Compumag Society Newsletter, Vol. 12, No. 1, pp. 2—9, 2005
- [13] Razek, A. A., Coulomb, J. L., Féliachi, M., Sabonnadière J. C.: *A Concept of an Air-Gap Element for the Dynamic Analysis of the Electromagnetic Field in Electric Machines*, IEEE Transactions on Magnetics, Vol. 18, No. 2, pp. 655—659, 1982  
DOI: 10.1109/TMAG.1982.1061898
- [14] Davat, B., Ren, Z., Lajoie-Mazenc, M.: *The Movement in Field Modeling*, IEEE Transactions on Magnetics, Vol. 21, No. 6, pp. 2296—2298, 1985  
DOI: 10.1109/TMAG.1985.1064185
- [15] Dular, P., Geuzaine, C., Ferreira da Luz, M. V., Sadowski, N., Bastos, J. P. A.: *Connection Boundary Conditions with Different Types of Finite Elements Applied to Periodic Conditions and to the Moving Band*, COMPEL - The international journal for computation and mathematics in electrical and electronic engineering, Vol. 20, No. 1, pp. 109—119, 2001  
DOI: 10.1108/03321640110359796
- [16] Sadowski, N., Lefèvre, Y., Lajoie-Mazenc, M., Cros, J.: *Finite Element Torque Calculation in Electrical Machines While Considering the Movement*, IEEE Transactions on Magnetics, Vol. 28, No. 2, pp. 1410—1413, 1992  
DOI: 10.1109/20.123957
- [17] Demenko, A.: *Movement Simulation in Finite Element Analysis of Electric Machine Dynamics*, IEEE Transactions on Magnetics, Vol. 32, No. 3, pp. 1553—1556, 1996  
DOI: 10.1109/20.497547
- [18] De Gersem, H., Ion, M., Wilke, M., Weiland, T., Demenko, A.: *Trigonometric Interpolation at Sliding Surface and in Moving Bands of Electrical Machine Models*, COMPEL - The international journal for computation and mathematics in electrical and electronic engineering, Vol. 25, No. 1, pp. 31—42, 2006  
DOI: 10.1108/03321640610634308
- [19] Salon, S. J., Schneider, J. M.: *A Hybrid Finite Element – Boundary Integral Formulation of the Eddy Current Problem*, IEEE Transactions on Magnetics, Vol. 18, No. 2, pp. 461—466, 1982  
DOI: 10.1109/TMAG.1982.1061891
- [20] Alotto, P., Bertoni, A., Perugia, I., Schötzau, D.: *Discontinuous Finite Element Methods for the Simulation of Rotating Electrical Machines*, COMPEL - The international journal for computation and mathematics in electrical and electronic engineering, Vol. 20, No. 2, pp. 448—462, 2001  
DOI: 10.1108/03321640110383320

- [21] Preston, T. W., Reece, A. B. J., Sangha, P. S.: *Induction Motor Analysis by Time-Stepping Technique*, IEEE Transactions on Magnetics, Vol. 24, No. 1, pp. 471—474, 1988  
DOI: 10.1109/20.43959
- [22] Perrin-Bit, R., Coulomb, J. L.: *A Three Dimensional Finite Element Mesh Connection for Problems Involving Movement*, IEEE Transactions on Magnetics, Vol. 31, No. 3, pp. 1920—1923, 1995  
DOI: 10.1109/20.376415
- [23] De Gersem, H., Weiland, T.: *Harmonic Weighting Functions at the Sliding Interface of a Finite-Element Machine Model Incorporating Angular Displacement*, IEEE Transactions on Magnetics, Vol. 40, No. 2, pp. 545—548, 2004  
DOI: 10.1109/TMAG.2004.824616
- [24] Rodger, D., Lai H. C., Leonard, P. J.: *Coupled Elements for Problems Involving Movement*, IEEE Transactions on Magnetics, Vol. 26, No. 2, pp. 548—550, 1990  
DOI: 10.1109/20.106375
- [25] Antunes, O. J., Bastos, J. P. A., Sadowski, N.: *Comparison Between Torque Calculation Methods in a Non-Conforming Movement Interface*, COMPEL-The International Journal for Computation and Mathematics in Electrical and Electronic Engineering, Vol. 27, No. 1, pp. 27—36, 2008  
DOI: 10.1108/03321640810836609
- [26] Rodger, D., Lai, H. C., Leonard, P. J.: *Coupled Elements for Problems Involving Movement*, IEEE Transactions on Magnetics, Vol. 26, No. 2, pp. 548—550, 1990  
DOI: 10.1109/20.106375
- [27] Buffa, A., Maday, Y., Rapetti, F.: *Calculation of Eddy Currents in Moving Structures by a Sliding Mesh-Finite Element Method*, IEEE Transactions on Magnetics, Vol. 36, No. 4, pp. 1356—1359, 2000  
DOI: 10.1109/20.877690
- [28] Henrotte, F.: *Handbook for the Computation of Electromagnetic Forces in a Continuous Medium*, International Compumag Society Newsletter, Vol. 11, No. 2, pp. 2—8, 2004
- [29] Arkkio, A.: *Analysis of Induction Motor Based on the Numerical Solution of the Magnetic Field and Circuit Equations*, PhD thesis, Helsinki University of Technology, 1987
- [30] Davey, K. R.: *Induction Motor Analysis—International TEAM Workshop Problem 30* [Online]. Available: <http://www.compumag.co.uk>
- [31] Agros2D - free finite element software [Online]. Available: <https://www.agros2d.org/>

# Consideration on road transport vibration simulation techniques for packaging testing purposes

**R. Pidl**

**Department of Applied Mechanics, Faculty of Mechanical Engineering  
Information Technology and Electrical Engineering  
Széchenyi István University  
9026 Győr 1 Egyetem tér, Hungary  
[pidlre@sze.hu](mailto:pidlre@sze.hu)**

**Abstract:** Transportation is essential for many logistics systems and vibration is one of the most critical physical circumstances on road causing numerous possible damage sources. One of the primary sources of these damages is often the broadband random vibration. This effect cannot be handled with formal mechanical models; therefore, vibration test simulation is essential for packaging testing. The current vibration systems use Power Spectral Density (PSD) functions to control the intensity of random signal in laboratory based on Fast Fourier Transformation (FFT). Naturally, the PSD frequency does not contain time series data making it hard to determine how long a given simulation should be performed. In this paper, mathematical and probability methods are presented that can be used for representing real vibration circumstances.

*Keywords: packaging, vibration, acceleration, PSD, simulation*

## 1. Introduction

The movement of vehicle platform during traveling is a very complex phenomenon and depends significantly on the current state of the track-vehicle system. The product-packaging system has to be designed for vibration environment in order to avoid transport damages. For the time being, this is not completely resolved. For example, in Germany the amount of transport damages is between 200 and 250 million EUR based on insurance data [1]. Majority of these are caused by the not properly designed product-packaging-cargo systems and their protecting functions, or during transport an extra effect hits the cargo on the platform, that could not be considered.

A non-adequate packaging could be a global problem causing millions of dollars of cargo damage, not counting the environmental effects. This way two separated options can be drawn. The first one is when the packaging is underestimated. The packaging cannot withstand the stress and the cargo is damaged, or even worse, when the non-adequate packaging causes accidents (also based on German insurance data: 12 death

yearly are caused by non-adequate packaging design and cargo securing). This topic contains also transport safety issue. The other possibility is the overprotecting of the product. It is expensive, the vehicles are not utilized optimally, causing thereby more traffic and economic impact – not only from traffic but also from the waste of the additional and unnecessary packaging. The task of the engineer is therefore to optimize the protection of the product to prevent and avoid damages and to minimize the cost and the amount of packaging materials together.

Shocks, vibrations from the track-vehicle system can be one of the primer causes of damages. This is why it is of utmost importance to simulate these stresses before transportation as exactly as possible. For the time being no totally perfect solution is available for this issue [2]. Over the last 50 years, the vehicle vibration simulations developed from simple mechanic instruments to state-of-the-art computer controlled vibration tables [3]. But even the most advanced model considers the vehicle cargo platform as a fix body, where the fact is that those platforms can bend for prolonged time, also behave as a flexible body. It also increases to the complexity of the problem that - besides the broadband frequency of movement- additional effects are present, namely prolonged and low frequency movements caused by braking, accelerating, etc. This effect is affected by the construction and is so complex that it cannot be fully modelled. The theoretic calculations, especially those without the use of computer, can have two degrees of freedom vibration system, whereas the platform is a vibration system with six degrees of freedom. Therefore, besides the theoretical calculations – that is simplified – laboratory simulations are also required for cargo planning [4]. The simulation of dynamic stress proposes many problems. It handles the platform as a fix body and cannot represent the movement correctly. With the use of the superposition principle, the real motion cannot be represented together with its longitudinal, vertical and lateral components [5]. The problem to be solved is what to choose as a relevant stress to be used for the protecting function design of the cargo [6].

## **2. Currently used vibration simulation methods**

### **2.1 Techniques**

Besides the standard procedures, a variety of alternative simulation methods also exist. In literature, 5 types of these methods can be identified [6] as follows:

- Time-based playback of recorded sign history
- Generating random vibration signal by normal distribution (Gauss simulation)
- Non-Gaussian distribution simulation:
  - non-stationarity simulation methods
  - transient event simulation
  - harmonic simulation

### **2.2 Standard procedures**

The first equipment of transport simulation was quite simple: a table is moved with eccentric teeth, simulating large shocks, where the table and the teeth are not in constraint connection. The upper dead point is maximized. This means practically the current U.S.

standard listed as ASTM D999-08 [7]. Repeating large shocks can be reproduced, but no real vibration effects could be simulated with it.

A better solution is the ASTM D3580 [8] and the corresponding ISO/IEC 60068-2-6 [9] standard vibration equipment with clean sinus acceleration signs. This equipment has hydraulic power transmission and the sinus vibration is performed in the frequency range of 1-100 Hz. The hydraulic actuator holds acceleration between 0.5 - 1g in the whole frequency range with decreasing trajectory amplitude with the rising of frequency. These apparatuses are controlled with trajectory steering. No computer aided control is required; inner electronics can handle it simply. The rate of frequency change (sweep) can be controlled separately in octave/min according to the standard. Also, according to the standard, the sweeping speed is 0.5-5 octave/min. The test has to be performed with upwards sweeping and after reaching the upper frequency limit, with downwards sweeping as well. Unfortunately, this standard is rarely used for the time being, despite the fact that the critic resonance stripes could be well determined with them. If random acceleration-time functions are considered on vehicle cargo platforms, it can be seen that they always contain harmonic sinus components. These components are coming from the not balanceable driven wheels and the actual rev of the engine. These harmonic components can cover a very broad frequency range, because they depend on the actual speed, the motor rev depending on accelerating and braking and the gear position, respectively. It must be noted here that diesel engine upper rev is much lower than Otto engines' upper rev, thus the 100 Hz upper frequency limit at diesel engines is excessive. If real transport environment were considered, the sinus sweeping should be parted to frequency ranges to simulate first gear, accelerating from 0-10 km/h, then second gear, speeding from neutral rev again, and so on, of course with the necessary deceleration and gear shift backs. This could be simulated with sine sweep with sweeping to a low upper frequency, then back to neutral rev and so on. In the packaging testing laboratory of the Széchenyi István University two types of electrodynamic vibration test machines are installed: MTS (Fig. 1.) and TIRA (Fig. 2.), where mentioned standards' tests above can be performed.



Figure 1. Servo-hydraulic vibration system



Figure 2. Electro-dynamic vibration system

It is obvious that the behaviour of the tested cargo is different in the frequency ranges during upward or downward sweeping. The explanation and reason for this phenomenon could be the late reaction of the test subject to various frequency changes, and in this instant the cargo moves away in reaction to the motion of the table and starts to bounce on the table. However, it must be stated here that the deterministic mechanical models typify the partly parallel, partly serial connected swinging parts built from springs and

absorbers as a swing system connected to each other. The functions are created for the theoretical excitation excluding the fact that separation could occur both in the road-wheel and in the platform-cargo connection in the frequency ranges. At the moment of separation, the force-excited swing system starts to vibrate in its own frequency – that frequency differs from the original exciting frequency. That continues until the separated cargo hits the vibration table again. At this moment the two separate, independently vibrating swing systems meet and neither their amplitude nor their frequency and phase are the same. This is critic, hence the hits could damage the packed product too. The other critical part of the sinus sweeping is where the exciting frequency meets the frequency of the cargo. This is called resonance and here 6-8 times the exciting acceleration amplitude affects the test subject. It is very complicated to determine however, whether this frequency exists in a given transport vehicle, and if it exists, how often. This harmonic sinus vibration test should be performed for sure, but in my opinion the test procedure should be changed.

Many standards exist for broadband, random excited vibration tests (ASTM D4169-16, MIL-STD-810F, ISO 13375:2003) [11-13]. For the time being these broadband, random excited vibration tests are the most widespread. These could be performed with both electrohydraulic and electrodynamic vibration tables, with computer calculated PSD-frequency functions from Fast Fourier Transformation where the upper and lower frequency limits and the PSD and RMS values in the various frequency ranges are determined. These functions were created after many measurements on transport vehicles and recorded for various times of the acceleration-time function and determined the PSD-frequency function with FFT and after many measurements a statistically representative sample was created where normal distribution of the PSD values were presumed [14]. The standard PSD characteristics must be added per frequency range to the control computer of these equipment and this computer creates random transitional situations, but during the full run time all such situations are created. These equipment are very complex and expensive, because they have to manage the current swing trajectory and current acceleration furthermore the control unit has to determine the actual PSD value simultaneously. A further question is the required duration of the simulation depending on the transportation distance. This is a very important practical question, because - especially in case of large distance transports- simulating the whole length is impossible and the PSD function will not excite real values but it will compress all the unique vibrations in the whole frequency range and the small bandwidth vibrations also [15]. It can be said that with the transforming of vibrations to frequency ranges the possibility of measuring in time range will be lost. Many testing laboratories realized this and the development of this method is in research focus for the time being. For the required test duration Basquin is suggesting the following model [6]:

$$\frac{t_j}{t_k} = \left( \frac{a_t}{a_j} \right)^k \quad (1)$$

where:  $t_j$  is the current transport duration,  
 $t_k$  is the test duration,  
 $a_t$  is the test intensity,

$a_j$  is the transport intensity,  
 $k$  can be freely chosen between 2-5.

The simulation problems erecting from the PSD frequency functions can be analysed with understanding the FFT, that is, the complex problematic of transiting from timelines to frequency lines (Fig. 3.).

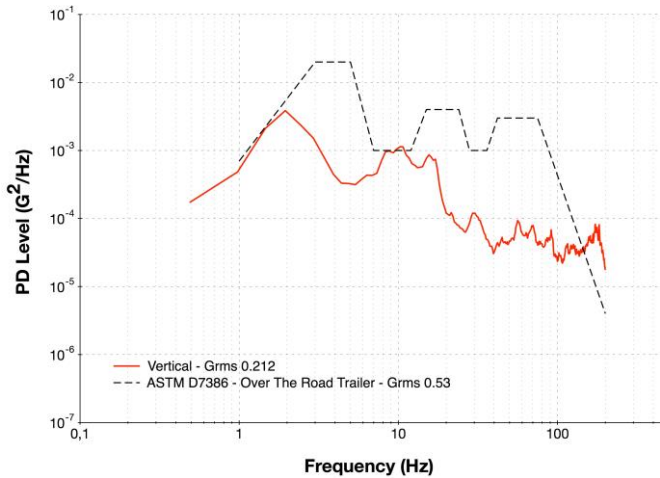


Figure 3. Field measured PSD frequency function compared to ASTM D4169-16 vibration standard method

## 2.3 Non- standard procedures

### 2.3.1 Simple playback of real recorded acceleration-time function

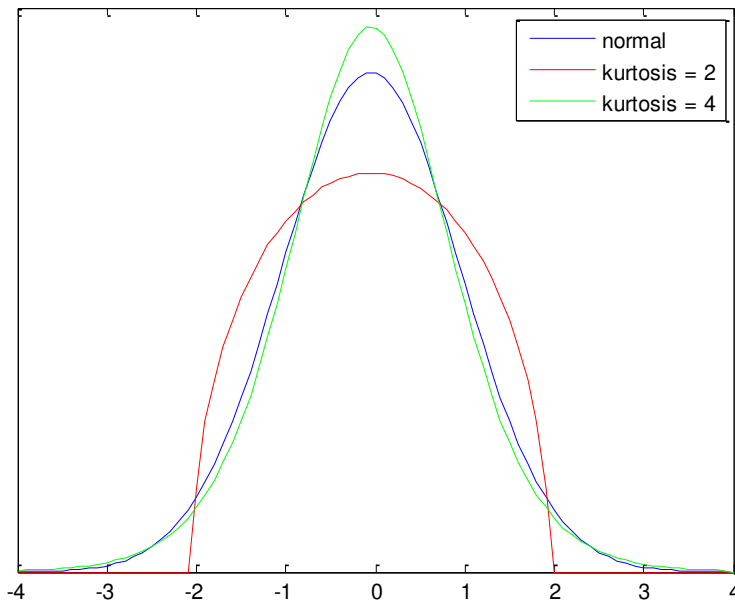
Computer controlled vibration machines offer the possibility to digitally record the acceleration-time function on a vehicle transporting a given cargo, then after input to the computer the machine can repeat it. The problem with this method that it is valid only for the given situation, other cargo or vehicle or driver or weather conditions could result in a completely different acceleration-time function. Furthermore, the test duration has to be the same as the transport duration. Because of these constrains, this method is not too widespread, but it has some advantages, for example, the transients during transport (road errors, railroad crossing, etc.) can also be recorded and used. Furthermore, the various transport environments (urban roads, motorways, industry roads) can be repeated according to the correct order.

### 2.3.2 Non-stationary and transients to FFT simulation, Gaussian distribution simulation

The FFT is one of the greatest inventions of mathematics from the last century [17]. It lowers the necessary operation time compared to discrete Fourier transformation, so this advantage should be used. But the Gaussian distribution used in FFT excludes the values outside the normal distribution at vibration tests. A method has to be found that includes

the values outside the standard deviation thus bias the normal (Gaussian) distribution function according to our aim.

Obviously, it is possible to adjust the probability density function of normal distribution with various probability calculation or mathematic statistic methods in order to avoid the loss of high intensity signs (even losing one is a problem), and still maintaining the test simulation intensity at normal level. One possible solution is to bias the Gaussian curve with the kurtosis calculation method, shown in Fig. 4. It can be proven analytically that in normal distribution the kurtosis value is 3, and if the kurtosis  $> 3$  it is called leptokurtic, if its equal to 3, mesokurtic and if kurtosis  $< 3$  it is called platykurtic, respectively. Hence normal distribution in the above case can be regarded as standard, the kurtosis values should be transformed by subtracting 3 from its value and measuring the excess kurtosis. This makes the kurtosis of normal distribution to zero, and all cases are either negative or positive.



$$Kurtosis = \frac{1}{T} \int_0^T \left[ \frac{a(t)}{\sigma} \right]^4 dt$$

Figure 4. The effect of various kurtosis values on the Gaussian curve

A debate is going on that which kurtosis value recreates the most exactly the original acceleration-time function for various transport solutions. Even the with kurtosis adjusted normal distribution-like distribution does not contain the non-stationers of the transport processes. This non-stationarity comes from road surface quality – even the slightest change results in a completely different acceleration-time function. Also, a cause is the constant change in vehicle speed. Other speed ranges are used on motorways, urban roads,

suburban roads, and all that affect the vibration during transport. Fig. 5/a. shows a field measured acceleration-time history in 40 seconds with the kurtosis value of 7, while Fig. 5/b. shows an acceleration-time history using by vibration systems' random generator with value of 3.

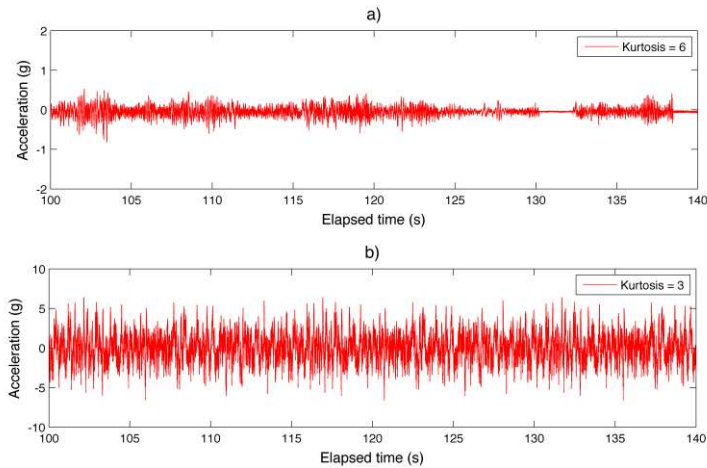


*Figure 5. Acceleration-time history, a) field measured signal displaying road surface errors, b) random signal using by vibration controllers in laboratory*

One possible solution to simulate road surface quality changes is to use leptokurtosis. Another possible solution for simulation non-stationarity could be the spectrum splitting, split the normal distribution to sequences, the Wavelet transformation and the use of Bayesian detection [19].

The major problem of the standard methods is that these exclude the transient events from the vibration profile, even though in practice the majority of cargo damages could be traced back to this unique, hard hit-type stresses [20]. The aim of the authors' doctoral thesis is a method for simulating these transient events on vibration equipment, and what type of acceleration-time functions those have in case of a railroad crossing or road surface damages. It has to be determined how many times these occur during a given transport and whether it should be included in the beginning or at the end of the simulation process. This leads to the packaging padding size decisions. It is without doubt that the viscoelastic characteristics of cushioning foams made from various polymer types are different, thus it has to be decided what the greater cargo damage causes: the big hit at the start of the test that annuls the elasticity of the foam letting the product vibrate freely or when the foam exhausted from the long vibration gets compacted and harder and hits the product with more excessive force than the not exhausted foam.

### **3. Analytical model for testing the effects of random non-Gaussian vibrations**

Obviously, the vibration tests' purpose is to protect the goods after vibration stress. In the model we presume that the product is a solid body protected on its eight corners with cushioning material (usually a polymer foam), held together with a box. It may not be considered as the material of the box. This system is applied to the vibration machine table. If the product is a solid body it can be characterized with its weight and geometric dimensions. The cushioning material will be replaced with parallel connected  $k$  spring constant and with  $c$  damping ratio. For the analysis of the system, the spring and damping characteristics should be known. In first iteration the  $k$  and  $c$  are presumed to be linear, that is not true in practice of course, but it can be used to determine the own frequency of the system with a vertical shock.

The motion equation will be the following [20]:

$$m(\ddot{u} + \ddot{z}) + c\dot{u} + ku = 0 \quad (2)$$

where:  $m$  [kg] is the product weight,  
 $k$  [N/mm] is the spring constant,  
 $c$  [N/mm] is the damping ratio,  
 $z$  [mm] is the total swing length of the vibration table (input),  
 $u = x - z$  [mm] is the motion of the product relative to the vibration table.

Parameter  $u$  can be calculated from the equation if  $m$   $c$   $k$  and  $z$  are known and then  $x$  can be calculated as  $\ddot{x} = \ddot{u} + \ddot{z}$ .

If such a system is dropped from a pre-defined height we can determine the peak acceleration with an accelerometer as the following:

$$\ddot{x}_{\max} = \left| \frac{2\zeta^2 - 1}{\sqrt{1 - \zeta^2}} \right| \exp\left( \frac{-\zeta\pi}{2\sqrt{1 - \zeta^2}} \right) v \omega \quad (3)$$

where:  $\zeta$  is the damping ratio,  
 $v$  is the vertical collision speed,  
 $\omega$  is the natural angular frequency.

If this test is performed on an actual package and the parameters are defined, the behaviour to vibration effects can be determined with numeric simulation. A possible simulation model is the MapleSim (Waterloo, Maple, Inc., Canada) software. This software is also capable of adjusting the Gaussian distribution PSD with kurtosis values 3, 5 and 7 [13].

With transporting test of the actual package, during which the vibration acceleration values were measured on the product itself, performing an FFT on the resulting acceleration-time function it was clear that the numeric simulation could determine the effecting acceleration of the product with good iteration by using a kurtosis value of 7.2.

That also means that by choosing 7.0 kurtosis value on the vibration table the original acceleration-time function can be reproduced.

#### **4. Summary**

During logistics processes, various external physical events affect the packed products. The product may tolerate these effects but excess external effects have to be handled by the protecting function of the sustainable packaging. From among these various external effects, this paper dealt with the random vibration occurred during transport and loading. In this paper first a review was performed about the currently used testing and calculation methodologies that are imperfect from many aspects. The formal models exclude even relevant effecting factors and laboratory testing cannot reproduce real world effects either. Of course, it has to be mentioned that real world effects also contain numerous random elements – question is when to consider something normal or above normal vibration effect. After many laboratory-testing methods had been chosen that could be regarded significant based on statistics analysis and after considering some safety factors, the real circumstances can be iterated well. The Gaussian distribution used for vibration testing simulation has to be altered. The best solution at hand is the use of Gaussian distribution with altered kurtosis. With altering kurtosis values a probability density function can be created that could reproduce the measured real function during laboratory testing quite well. This study also mentioned that the currently neglected harmonic excited vibration tests should be introduced in an altered form. With this method, the determination of the natural own frequency of the product-package system could be compared with the affecting vibration frequencies of transport and material handling – and if these do not match, then additional protection is no needed. On the other hand, if in some frequency bands the functions match, either with the change of product construction or packaging damping system adjustment the damaging vibration effects could be minimized. At the end of the paper a possible calculation method was presented, that based on the above experiences could give a starting value for the characteristics of the cushioning material that could shorten the iteration time of the cushioning design process.

#### **References**

- [1] Röbbisch K: Transportsicherer profitieren 2014 von geringen Schadenquoten, IUMI-Konferenz, 2015 Berlin
- [2] Rouillard V, Sek M: Creating transport vibration simulation profiles from vehicle and road characteristics, *Packaging Technology and Science* 2013; Vol. 26, No. 2: pp. 82–95.
- [3] Harris C, Piersol A: *Harris' shock and vibration handbook*, (2001).
- [4] Böröcz P: Analysing the functions and expenses of logistics packaging systems, *Proceedings of FIKUSZ 2009: Symposium for young researchers*, Budapest, Hungary, 2009, pp. 29-39.
- [5] Charles D: Derivation of environment descriptions and test severities from measured road transportation data, *Journal of the IES* 1993; Vol. 36, No. 1, pp. 37–42.
- [6] Lepine J, Rouillard V, Sek M: Review on Road Vehicle Vibration Simulation for Packaging Testing Purposes, *Packaging Technology and Science*, 2015, DOI:10.1002/pts.2129, pp 672-682.

- [7] ASTM D999-08: Standard Test Methods for Vibration Testing of Shipping Containers, ASTM International: West Conshohocken, PA, 2008. DOI: 10.1520/D0999-08.
- [8] ASTM D3580-95: Test Methods for Vibration (Vertical Linear Motion) Test of Products, ASTM Standard: West Conshohocken, PA, 2010; 4. DOI: 10.1520/D3580-95R10.
- [9] IEC-60068-2-6: Environmental Testing – Part 2–6: Tests – Test Fc: Vibration (sinusoidal), International Electrotechnical Commission, 2007.
- [10] Barbosa RS: Vehicle Vibration Response Subjected to Longwave Measured Pavement Irregularity, *Journal of Mechanical Engineering and Automation*, 2012, pp 17-24.
- [11] ASTM D4169-12: Standard Practice for Performance Testing of Shipping Containers and Systems, ASTM International: West Conshohocken, PA, 2016, DOI: 10.1520/D4169-16
- [12] MIL-STD-810 F: Environmental Test Methods and Engineering Guides. Department of Defense Test Method Standard, USA, 2000.
- [13] BS EN ISO 13355:2003: Packaging, Complete, Filled Transport Packages and Unit Loads. Vertical Random Vibration Test, BSI: London, UK, 2002; 16.
- [14] Böröcz P, Singh SP, Singh J: Evaluation of Distribution Environment in LTL Shipment between Central Europe and South Africa, *Journal of Applied Packaging Research*, Vol. 7, No. 2, 2015, Paper 3.
- [15] Shires D: On the time compression (test acceleration) of broadband random vibration tests, *Packaging Technology and Science* 2011; Vol. 24, No. 2., pp. 75–87.
- [16] Steinwolf A, Cannon III WH: Limitations of the Fourier Transform for Describing Test Course Profiles, *Sound and Vibration*, 2005, pp. 12-17.
- [17] Dongarra J, Sullivan F, Guest Editors' Introduction: The Top 10 Algorithms, *Computing in Science & Engineering*, Vol. 2, No. 1, pp. 22-23, 2000, DOI:10.1109/MCISE.2000.814652
- [18] Böröcz P, Vastag Gy: Good Vibrations: Lessons from Packaging for the Global Supply Chain.", *POMS* 2015, 1318.
- [19] Böröcz P, Singh SP: Measurement and Analysis of Vibration Levels in Rail Transport in Central Europe, *Packaging Technology and Science*, 2016, Early View, DOI:10.1002/pts.2225
- [20] Hosoyama A, Saito K, Nakajima T: Effectiveness of Stationary Non-Gaussian Random Vibration Testing and its Influence on Packaging, *Proceedings of 26th IAPRI Symposium on Packaging* 2013, pp 86-97.

# Individual Test Rig for Measuring the Creep Behaviour of Corrugated Board for Packaging

V. Köstner<sup>1</sup>, JB. Ressel<sup>2</sup>, B. Sadlowsky<sup>1</sup>, P. Böröcz<sup>3</sup>

<sup>1</sup>Institute for BFSV  
Ulmenliet 20, 21033 Hamburg, Germany  
Phone: +49 40 42875-6046

<sup>2</sup>University of Hamburg, Department of Wood Science  
Mittelweg 177, 20148 Hamburg, Germany  
Phone: +49 40 42838-0

<sup>3</sup>Széchenyi István University, Department of Logistics and Forwarding  
Egyetem tér 1, 9026 Győr, Hungary  
Phone: +36 96 503-400  
e-mail: boroczp@sze.hu

**Abstract:** Corrugated board is one of the most important and most popular packaging materials worldwide for transporting goods. Due to its hygroscopic behavior, it has a tendency to creep when subjected to stress under a constant load, which can ultimately result in loss of strength, with possible damage to products. The creep behavior of corrugated board is still a largely under-researched area. This paper attempts to examine the long-term behavior of corrugated board during use more precisely than before, and presents the first step and results of the research process. For the measurement, a compact and high-precision individual test rig was developed and used, in order to reduce the side effect of coupled systems, that is, to avoid their mutual influence. This paper successfully presents results reproducible with the described test rig apparatus for determining the creep behavior of corrugated board. It will be continued to publish further results of the research in the near future.

**Keywords:** *corrugated board, creep behaviour, packaging material*

## 1. Introduction

For the EU-28, in 2013, 40 % of main packaging materials were paper-based packaging, including corrugated board as the most popular and well-known transport packaging [1]. Thanks to the special construction of corrugated board relatively high strength features can be achieved, coupled with low weight. The only Achilles tendon or disadvantage of corrugated board is its hygroscopic behavior. If corrugated board packaging encounter with high relative humidity (RH), it loses up to 50 % of its strength [2-5].

Various international standards (FEFCO, ISO, ASTM, TAPPI) use testing practices to measure the mechanical characteristics of paperboard, but these are mostly limited to short-term measurements aimed at assessing compression strength [6-9]. Historically, the corrugated board industry has established the nature and scope of compression strength measurements. Experts and researchers believe that measurement results derived from box compression test (BCT) allow them to evaluate the compressive behavior of boxes. However, it needs to be noted here that compression strength measurements were developed primarily for quality control purposes. Furthermore, large production volumes do not allow any of the test methods to be applied for a relatively long duration.

The current standards and guidelines do not include a quality standard that would take this type of long-term load into account. Furthermore, it is difficult to give an appropriate estimate of the ability of corrugated board to cope with in-transit stress. In practice, therefore, safety factors are used to take stresses such as high RH and transport loads into account. This can lead to significant overpacking, and consequently a waste of resources. However, if the product-package system is under designed, that can result in packaging failure with a possible risk of product damage [10-11]. T. Trost and J. Alftan published in 2016 the current state of the scientific knowledge about the standards for optimizing corrugated board packaging for exporting industry. There they illustrate the lack of information in the areas of the effects of creep and varying climate conditions [12].

Although previous studies have been done on the mechanical behaviors of these packaging structures under static compression [13-16], they mainly focused on the mechanical behaviors of a corrugated board box itself. Other papers presented results and brief reviews of designing and modeling the stackability of cardboard boxes using a finite element method (FEM) [17-18]. The results of these tests can be applied as input data for decision support models and processes aimed at selecting the right protective packaging system [19]. However, it is well known that the long-term distribution environment and storage can affect the real strength of packaging, especially in the case of corrugated paper packaging [20].

The aim of this paper is to develop a new test rig for the examination of creep behavior of corrugated board on edge crush test (ECT) specimens for laboratory use to better exploit the material's potential. The long-term strategy of the experimental research is to create a guideline for packaging producers and engineers of corrugated board, firstly to prevent overdesigning and secondly to avoid product damage due to failure of the paperboard packaging.

## **2. Background and Methods**

In 1963, McKee established a connection between the ECT value, bending stiffness (BS) and BCT value of corrugated board [21]. The result of this research led to the McKee formula. Recently, this formula is widely used to calculate the BCT value of packaging made of single-walled corrugated board from its ECT value and BS [21-23]. Based on the assumptions of McKee, research into a possible correlation between long-term ECT and long-term BCT values was carried out at the Institute for BFSV at the Hamburg University of Applied Sciences.

As a result of the research project, called “Development of Test Standards relating to the creep Behavior of heavy-duty Corrugated Board for determining the Performance of Boxes manufactured therefrom” (DLR project no. 01FS10018), a creep test rig was designed to determine creep rates in specimens for edge crush resistance (ECT specimen: 25x100 mm). Figure 1 shows the schematic representation of the creep test rig with dimensions of 1060x400x400 mm.

To observe the edge crush resistance and creep behavior of corrugated board the test rig was designed with full consideration of the requirements of ISO standards such as ISO 3037:2013 and ISO 204:2009. These standards specify methods for uninterrupted and interrupted creep tests of metallic materials and the unwaxed edge method for determining the edgewise crush resistance of corrugated board. The basic frame 1 includes four test units 2-5, for simultaneously testing four ECT specimens; this can be seen in Figure 1. The test unit consists of a mounting plate 6 and a specimen plate 7. The test specimens 8 sit on the specimen plates during testing. The weights 9 required for the test are arranged on the mounting plates. Digital measuring sensors 10 are mounted on each test unit for measuring displacement. The lift station 11 and the motor 12 move the test units up and down.

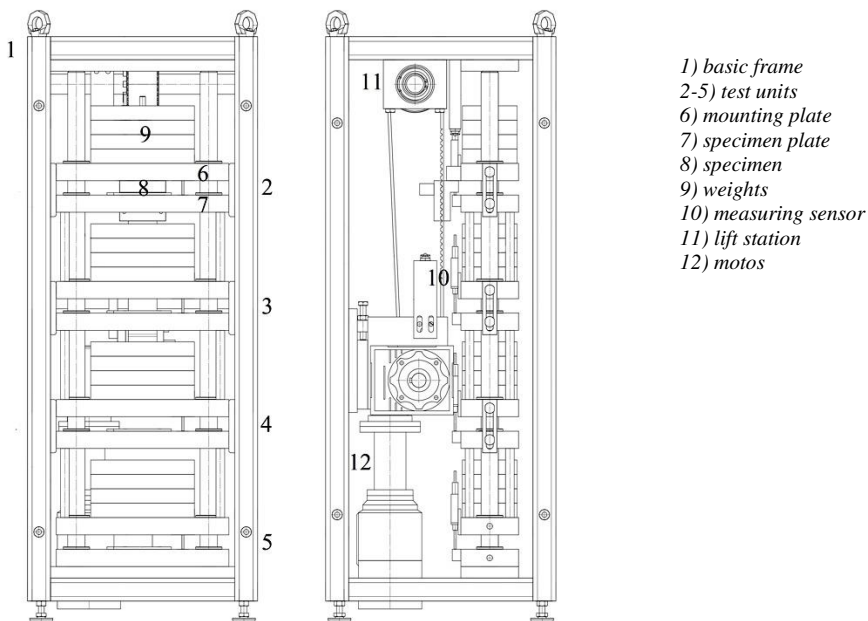


Figure 1. Stacked test rig

Advantages and disadvantages became clear when using the test rig. The cascade-like construction of the test rig makes it possible to test four specimens at a time. However, due to the combined weights of individual test units it is seldom possible to use the first and fourth level. The construction and size of the test unit severely restrict the dimension

of test specimen. In addition, no more than two displacement transducers can be attached per test level. It is also impossible to rule out an influence exerted by the failure of a specimen and transmission of any vibrations associated with this to the other specimens.

### 3. Requirements of a new test rig

When developing the individual test rig for laboratory use, two areas should be concentrated on: the construction of the test rig and its operating principle. The aim of this research is to ensure the accuracy and reproducibility of the test. The individual test rig has been designed for laboratory use. Small dimensions and a low net weight are essential for ensuring that the rig can be handled manually by one person. At the same time, it is necessary to adhere to the required load range: the minimum load on the specimen is 10 kg, and the maximum is 120 kg. The individual test rig must enable highly accurate measurements. Due to its construction and the high positioning accuracy required the test rig must be designed in such a way that the specimen is loaded in parallel. It is essential that the weights be mounted on the individual test rig rigidly and without any play to prevent uneven loading.

#### 3.1. Individual test rig

Figure 2 illustrates the schematic representation of the individual test rig, without additional weights. The weight and dimensions of the individual test rig are 40 kg and 315x315x680 mm. The test setup essentially consists of two plates precisely parallel in their planes, which can be moved toward each other by means of four guide columns. The four guide columns, which are supported on linear ball bushing bearings, allow the weights to be mounted rigidly and without play. They also ensure the parallel loading of the specimen.

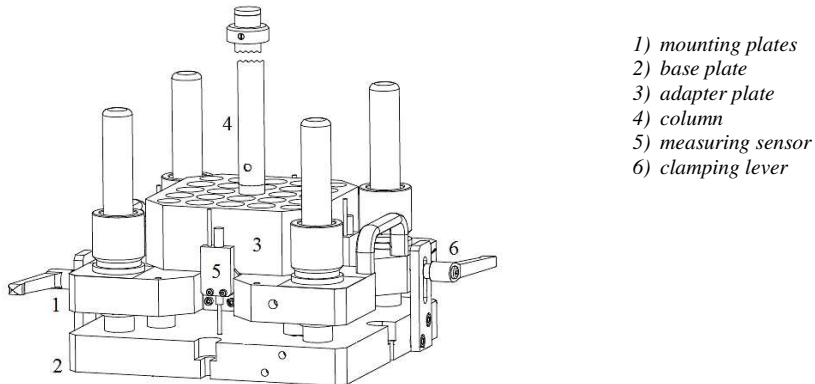


Figure 2. Individual test rig

When starting the test, the upper plates, known as the mounting plates 1, are raised and fixed in place by means of the corresponding clamping lever 6. The ECT specimen is placed centrally in the test chamber between the base plate 2 and the mounting plate. After carefully releasing the clamping lever, the mounting plate is slowly lowered onto the specimen. The weights can be mounted on the adapter plate 3 via a column 4. The special setup ensures the safe and stable placement of the weights. Digital measuring

sensors 5 are mounted on all four sides of the test rig to record the changes in distance during the measurement. All parts of the individual test rig are made of stainless steel to prevent corrosion.

### **3.2. Commissioning**

Commissioning of the individual test rig involves the following three areas:

- Measurement of parallelism,
- Determination of the dead load,
- Comparative tests.

The parallelism of the test plates is of extreme importance for accurately measuring creep rates in ECT specimens. It is essential to check parallelism, especially when the aim is to develop a new test method for generating comparable and reproducible creep rates in ECT specimens. Gauge blocks were used to determine the parallelism of the test plates at eight measuring points. The results of the parallelism measurement showed that the displacement on all points is 20.01 millimeters. Thus, there is no difference in the parallelism of the test plates.

Determining the dead load of the specimen is essential for designing the test loads correctly. In this case, a previously calibrated load cell was placed between the two test plates. The load cell then recorded the arising load. The result of the measurement revealed that the dead load of the specimen was 20 kg; twice the required minimum load of 10 kg.

### **4. Tests and results**

Comparative tests were conducted to assess the accuracy of the test rig. Creep tests were performed on ECT specimens using both test rigs. The subject of the observation was wet-strength, triple-wall corrugated board (DIN 55468-1:2015-06 2.96 heavy-duty board). The examinations were carried out in a climate chamber, simulating an eight-hour cyclical climate with a constant temperature of  $23\pm 2$  °C and RH rise and fall cycle stages to  $50\pm 5$  and  $90\pm 5$  % every three hours (Figure 3 blue graph). Figure 3 illustrates the result of a creep measurement of the individual test rig. The long-term ECT values diagrammed as a function of time and the creep deformation rate.

The red graph forms the creep deformation of the sample. Due to the superposition of the swelling behavior and the creep caused by the pressure load, creep deformation increases in the drying phase and decreases in the penetration phase [24]. The mean creep rate (0.006 mm/h) represents creep deformation (height reduction) as a function of time in the secondary phase of the creep process. At the time of its failure (134 h), the specimen suffered a significant loss of strength and practically collapsed. The criterion for specimen failure was a height reduction of more than 0.5 mm in 30 seconds. The experimental results of all measurements are shown in Figure 4.

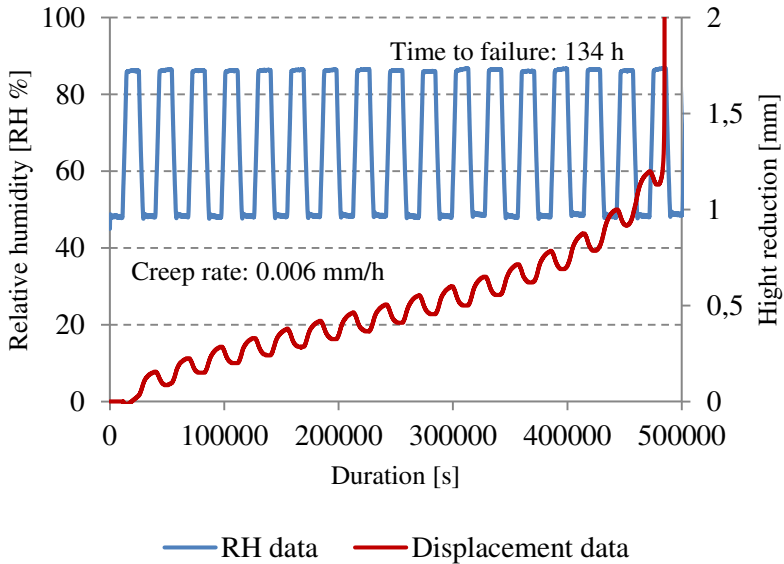


Figure 3. ECT long-term measurement tested with the individual frame

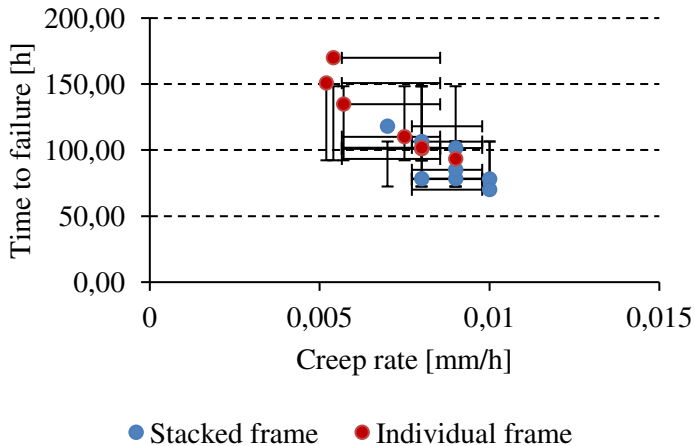


Figure 4. Results of the comparative measurements

Observing the results, it is noticeable that the creep rates and lifetimes generated by the two test rigs differ, considering the variances of the results. Although the average creep rates of both test rigs - stacked frame  $0.0088 \pm 0.001$  mm/h; individual frame  $0.0071 \pm 0.0014$  - seem to be similar, the deviation between the time to failure results of both test rigs - stacked frame  $89.5 \pm 17.04$  h; individual frame  $120.3 \pm 28.05$  h - is significant high. To what extent the deviation can follow from the natural fluctuation of the properties of

corrugated board is currently unknown. Additionally, due to the novelty of the measurement it is not possible to assess measurement errors based on the new type of measurement method for creep rates on ECT specimens. Further tests are intended to examine the extent to which external factors influence the values measured.

Considering the results of both test rigs together despite the deviation a linear relationship between the creep rate and the time to failure can be established (Figure 5). The coefficient of determination confirms the assumption. The higher the creep rate, the lower the time to failure.

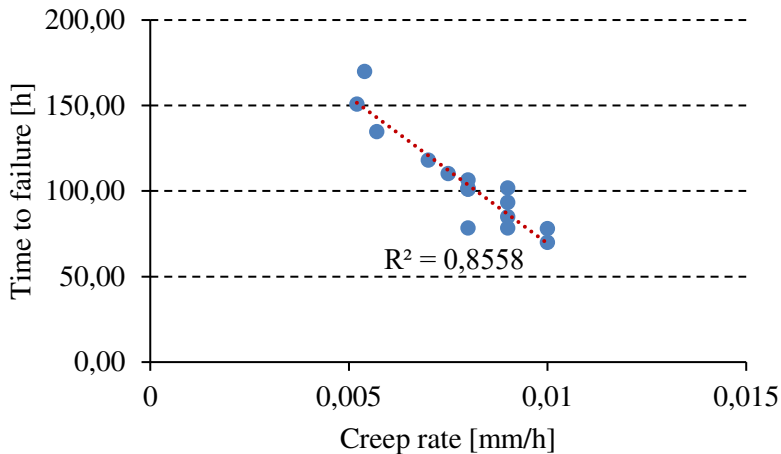


Figure 5. Results of both test rigs

## 5. Limitations

The individual test rig enables the examination of creep rates in ECT specimens in laboratories and can be controlled by one person due to its compact design and simple handling and operation. The special setup enables the examination of specimens of different heights and geometries. A disadvantage, however, is that due to the superstructures the minimum load on the specimen is 20 kg. Also, only one specimen can be tested at a time. The digital measuring sensor enables the recording of measured values up to 5  $\mu\text{m}$ . The creep rate was unknown when the test rig was designed. While a creep rate of 8  $\mu\text{m}$  can be mapped with the digital measuring sensor, it is not possible to assess the measurement error which may arise thus. In further tests, it will be necessary to examine the measurement error and the possible impact of external factors on the result. Readers of this paper, therefore, are advised to exercise caution when making direct comparisons with results from other research.

## 6. Conclusion and outlook

Based on the results of this study the following conclusions can be drawn. Using the newly developed, high-precision individual test rig reproducible results can be obtained. Comparison with the stacked test rig gave different creep rates and lifetimes, considering

the variances of the results. This variance should be investigated in more detail during further tests. In addition, as a next step, our research will focus on those factors, which can directly influence the measurement.

A new research project deals with the calculation of climate-dependent creep behavior with speed-dependent short-term tests. Thereby, various long-term tests concerning the BCT, BS and ECT will be performed. The results will be transmitted to a computer-aided calculation model under finite elements method (FEM). Subsequently the results of the FEM will be verified by short- and long-term test. Finally, it should become possible to use time- and money-saving short-term tests to estimate the long-term behavior of corrugated board. Hence, in the future, we might be able to utilize the potential of this packaging material better, prevent transport damage and protect the environment.

## References

- [1] EUROSTAT, European Statistical Database 2013, Development of the share of main packaging material, [http://ec.europa.eu/eurostat/statistics-explained/index.php/File:Development\\_of\\_the\\_share\\_of\\_main\\_packaging\\_materials\\_EU-27,\\_2005–13.png](http://ec.europa.eu/eurostat/statistics-explained/index.php/File:Development_of_the_share_of_main_packaging_materials_EU-27,_2005–13.png) [accessed 11 Jan 2017]
- [2] Dimitrov K, Heydenrych M. Relationship between the ECT-strength of corrugated board and the compression strength of liner and fluting medium papers, *Southern Forests* 2009; 71 (3): 227-233. DOI:10.2989/SF.2009.71.3.7.919
- [3] Niskanen K. *Mechanics of Paper Products*. Berlin/Boston, Walter De Gruyter, 2012.
- [4] Twede D, Selke S. *Cartons, Crates and Corrugated Board: Handbook of Paper and Wood Packaging Technology*, DEStech Publications, Inc., 2005.
- [5] Whitsitt WJ, McKee RC. Effect of relative humidity and temperature on stacking performance. Project 2695-9, Summary Report to the Technical Division of the FKBI Inc., 1972.
- [6] Test Method TAPPI T804 (om-12): Compression test of fiberboard shipping containers, 2012.
- [7] ASTM D642 – 00: Standard Test Method for Determining Compressive Resistance of Shipping Containers, Components, and Unit Loads, 2010.
- [8] FEFCO TM 50, FEFCO Testing Method Determination of the Compression Resistance of corrugated fibreboard containers, 1997.
- [9] ISO 12048 - Complete, filled transport packages – Compression and stacking tests using a compression tester, 1994.
- [10] Hiller B. Predicting the long-term mechanical behaviour of corrugated cardboard packaging based on speed rate controlled short term tests. *Proceedings of Progress in Paper Physics Seminar Conference*, pp. 65-70. Darmstadt, 2016.
- [11] Sadlowsky B., Ressel J. B., Reimers W., Köstner V.: Vorhersagbarkeit des Leistungsvermögens von Schachteln aus Wellpappe (FEFCO 0201) mithilfe des ECT-Langzeitwertes. *Holztechnologie* (in English: Predictability of the Performance of Corrugated Boxes (FEFCO 0201) by using the long-term ECT-Value), Nr.55, S. 30-35, 2014.
- [12] Trost T., Alftan J.: Standards for optimizing corrugated board packaging for exporting industry – A feasibility study. *Innventia Report No.: 730*, January 2016.

- [13] Aboure, Z, Talbi N, Allaoui S, and Benzeggagh M: Elastic behavior of corrugated cardboard: experiments and modelling. *Composite Structures*, Vol. 63, No. 1, pp. 53-62, 2004. DOI: 10.1016/S0263-8223(03)00131-4
- [14] Sek, M. A, Kirkpatrick J: Prediction of the cushioning properties of corrugated fibreboard from static and quasi-dynamic compression data. *Packaging Technology and Science*, Vol. 10, No. 2, pp. 87-94, 1997. DOI: 10.102/(SICI)1099-1522(199703/04)10:2<87::AID-PTS389>3.0.CO;2-L
- [15] Marcondes J. A: Effect of load history on the performance of corrugated fibreboard boxes. *Packaging technology and science*, Vol. 5, No. 4, pp. 179-187, 1992. DOI: 10.1002/pts.2770050403
- [16] Böröcz P. Measurement and Analysis of Deformation Shapes on Corrugated Cardboard Logistical Boxes under Static and Dynamic Compression, *Acta Technica Jaurinensis* 2015, (8)4, 320-329. DOI:10.14513/actatechjaur.v8.n4.389
- [17] Talbi N, Batti A, Ayad R, Guo Y. An analytical homogenization model for finite element modelling of corrugated cardboard. *Composite Structures* 2009, 88(2), 280-289, 2009. DOI:10.1016/j.compstruct.2008.04.008
- [18] Biancolini ME, Brutti C, Porziani S. Corrugated board containers design method. *International Journal of Computational Materials Science and Surface Engineering* 2010, 3(2), 143-163, 2010. DOI: 10.1155/2014/654012
- [19] Mojzes Á, Böröcz P. Decision Support Model to Select Cushioning Material for Dynamics Hazards During Transportation. *Acta Technica Jaurinensis* 2015, 8(2), 188-200. DOI:10.14513/actatechjaur.v8.n2.369
- [20] Böröcz P. Analysing the functions and expenses of logistics packaging systems. *Proceedings of FIKUSZ 2009: Symposium for young researchers*. Budapest, Hungary, 2009, Budapest Tech, 2009. pp. 29-39.
- [21] McKee R.C., Gander J.W., Wachuta J.R.: Compression strength formula for corrugated boxes. *Paperboard Packaging* 1963, 48 (8), 149-159.
- [22] Whitsitt, W. J.; Gander, J. W.; McKee, R. C.: Stacking behavior of boxes and corrugated board - A Summary Report of the Technical Division of the FKBI Inc., Project 1108-30, 12.04.1967
- [23] Whitsitt, W. J.; Gander, J. W.; McKee, R. C.: Effect of box dimensions and combined board creep life on box creep life - A Summary Report to the Technical Division of the FKBI Inc., Project 2695-2, 15.11.1968
- [24] Wagenführ A, Scholz F. *Taschenbuch der Holztechnik* (in English: Paperback of wood technology), Carl Hanser Verlag, München, 2008.

# Recycling of Mineral Water Bottles with Chemical Foaming

V. A. SZABÓ, G. DOGOSSY

Széchenyi István University, Department of Materials Science and Technology  
H-9026, Győr, Egyetem tér 1, Hungary  
Phone: +36 96 503 400  
e-mail: szabpanka@gmail.com; dogossy@sze.hu

**Abstract:** Today, in the field of packaging technologies there is an increasing amount of one-way polymer materials. Such materials after their short lifecycle are disposed, and such pose a serious environmental impact. However, PET is a good quality technical plastic; the recycled use must be provided. In our research, we have examined the recycled material of mineral water bottles. Chemical foaming of recycled polyethylene terephthalate (rPET) was applied for quality increased reusability. Significant results were achieved in terms of mechanical properties at specific mixtures of chain extender and impact resistance enhancer, at the foaming state of the injection moulding.

**Keywords:** rPET; recycling; chemical foaming; chain extender; polymer foam

## 1. Introduction

In the 1950's the consumption of fossil based raw materials rapidly grown along with the use of energy carriers. This attracted the rapid growth of the plastics industry. In 1970 the polyethylene terephthalate (PET) has been released and soon began to dominate the market for liquid foods packaging; consumer habits have changed. Due to low production costs, low weight, good optical properties and gas tightness PET has outperformed glass.

Due to the widespread use, PET waste will be projected to reach 29 million tonnes a year by 2018. As an effect of its mechanical and chemical properties, its resistance to chemicals and radiations is outstanding. At the same time this results in the natural decomposition of more than 450 years [1].

In this research work, technical properties of the PET will be presented that have become waste, in order to expand the possibility of secondary utilization. PET that has been discarded is still a good quality technical plastic; that can prove to be a major player in the future of raw materials.

During the production of the bottles, the preforms are placed in a stretching blower that warms them in a formable state in seconds. They are stretched longitudinally with a rod, and at the same time air is blown at high pressure, pushing the plastic to the bottle-shaped

metal mould wall. After the cooling, the shaping process is carried out. When the bottles are recycled, the chain structure of the PET is broken. The primary goal is to reverse the process, to improve the mechanical and physical properties of the recycled substance [2]. Various natural and synthetic raw materials were examined as to how effective they can be applied as chain extenders. During this work, the chosen manufacturing technology is injection moulding; by the change of the technological parameters of the moulding the change on the internal structure of the product is examined. The goal is to produce a low density material with specific mechanical properties. An examination for the automotive utilization of the raw material created, taking into account the wreckage directive (ELV Directive 2000/53 / EC). The aim of the research is partly environmental protection and partly the innovative technical raw material production [3].

### 1.1. Polyethylene terephthalate

Polyethylene terephthalate is a poly-condensation product of terephthalic acid and ethylene glycol (Fig. 1). It is currently considered the largest raw material for fibre manufacturing. Under nitrogen atmosphere, in the presence of Zn, Co, Mn acetate, dimethyldiphtalene with ethylene glycol is trans-esterified. During the reaction, the formation of the polymer is mainly due to gradual depletion.

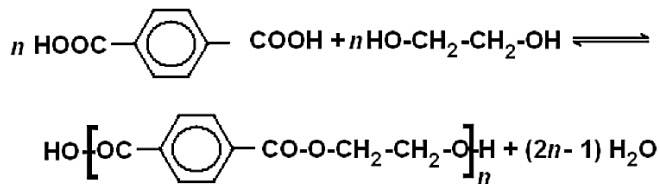


Figure 1. Equation of the production reaction of PET [4]

PET has high mechanical strength and high heat resistance, which is why crystalline technical plastics are typically used for fiber forming. Its resistance is very high; it is oil, grease, petrol and chemical resistant. Its radiation resistance and weather resistance are also good. Its negative property is to dissolve the alkali, phenol, cresol and its derivatives and destroy the structure of the oxidizing acids [4].

### 1.2. Manufacture of PET re-granulate

The main purpose of selective waste collection is to recycle. Only low-pollutant PET waste can be used for recycling. The recovery of the right raw material for recycling begins with selective waste collection.

Recycling of uncleaned and dry bottles is expensive. It would be an important expectation that we teach children what bottles can be collected at a young age. For example, in the acidic medium, the PET molecules cannot be degraded. Bases catalyse the degradation of PET molecules. Thus, the acetic and hydrochloric acid bottles in the waste bin will also prevent recycling of other bottles that come into contact with it. One of the regeneration steps of PET mills is cleansing and washing with water. The amount of water can be reduced by appropriate drying, and most be reduced because the presence of water reduces the average molecular weight of the polymer due to hydrolytic reactions.

PET mills process material in chemical and mechanical methods. Chemically, partial or complete depolymerisation is performed by the addition of water, ethylene glycol and methanol.

- PET mills + water → ethylene glycol and terephthalic acid
- PET mills + ethylene glycol → bis (hydroxyethyl) terephthalate
- PET mills + methanol → dimethyl terephthalate - is formed.

For mechanical processing, the regrind is cleaned, dried and then processed as a thermoplastic, in a melted state [5].

The injection moulding of high quality components from recycled PET is complicated by several factors. During recycling, thermal and shear stresses cause significant degradation, this can be further enhanced by possible contaminants and moisture content. Process-ability is a function of moisture content and should therefore be kept below 0.004%.

As a consequence of recycling, it is a serious problem that its mechanical properties are deteriorating [6,7].

This research is focused on the development of secondary raw materials with recycled PET foaming.

### **1.3. Foaming**

Under the term polymer foam, we mean a biphasic system in which statistical distributions of variable gas bubbles are embedded in a polymer matrix. Almost all thermoplastic polymers are suitable for making a foamed product. The foaming processes can be classified into three main groups: mechanical, physical and chemical.

During chemical foaming, the foaming agent forms a gas that foams the plastic structure. Foaming is started after mechanical stirring of the blowing agent. The process is supported by heat transfer. The formation of the foam structure is followed by forming and solidification. During the chemical reaction, various decomposition products are formed (eg. CO<sub>2</sub>, ammonia, water) [6].

Chemical blowing agents are organic or inorganic solids that decompose in a high temperature melt. Their solid decomposition products act as nucleus. In addition, large quantities of gas are generated. The gas bubbles formed at the nucleus in the coolant melt and form cells.

In the experiment, we combined the traditional injection moulding technology with the breathing- mould technique. The injection moulding cycle of the foamed specimens is as follows:

1. The mould closes.
2. The injection unit closes, connects to the injection-side of the mould.
3. The melted polymers is injected to the mould.
4. Holding pressure is maintained for 3 seconds.

5. Plastification of the materials for the next cycle.
6. The injection unit opens.
7. Mould breathing (the mould opens until 0.3 mm).
8. Cooling for 20 seconds.
9. The mould opens.
10. Ejection of the specimen.

#### 1.4. PET foaming

During PET foaming attention must be paid to the material drying, as due to hydrolysis the internal viscosity of the melt decreases; as a direct result the proper pressure at the nozzle is not formed. Foam stability is worsened, the distribution and size of the bubbles will not be adequate Cells cannot hold their spherical shape; larger diameters are torn off, causing poor surface quality. This phenomenon is also present in the recycling of rPET, which is a serious problem as the raw material and the quality of the finished product also deteriorate.

In the case of the study, PET re-granulate was dried for 12 hours at 140 °C. This is due to the humidity of the raw material; it has to be less than 0,004% for injection moulding. Chain extensions to the base material are added in addition to the chemical foaming agent. This process connects chains and improves mechanical properties and increases viscosity [8] (Fig. 2).

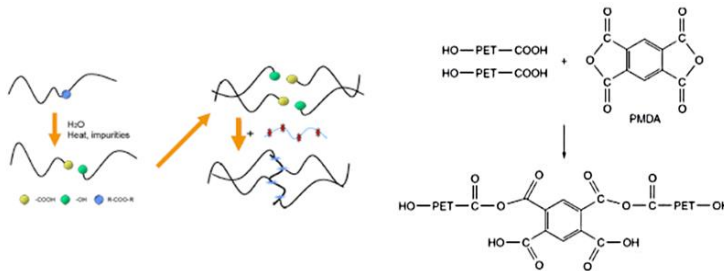


Figure 2. The principle and actual operation of the chain extension additive [6]

#### 1.5. Injection moulding

One of the most productive processing technologies is injection moulding; this process typically produces thin-walled products ranging from a few millimetres to several meters in length [8].

In the case of chemical foaming moulding, structural foam is produced because the shell of the product which is in contact with the wall of the tempered tool is generally solid [9]. Towards the core the foamed proportion increases. As to the size of cells, it can be observed that the cell diameters are larger in the middle of the product. During the chemically-foamed injection moulding process, self-closing nozzles must be used and greater compression pressure to prevent the material from foaming during plasticization.

## 1.6. Breathing-mould technique

In order to achieve the appropriate foam level, the pressure differences can be influenced by the mould opening or breathing tool technique. During this process, the polymer mixed with the blowing agent is injected into the mould cavity where the compact surface layer of the piece is formed during the cooling. Then, with the minimal opening of the tool the space increases and the pressure decreases, so that the still molten material is foaming. The tool opening depends on the setting of the tool cavity and the injection moulding machine. In the experiments, a 0.3 mm opening of the mould was used to produce the test specimens [10] (Fig. 3).

## 1.7. Aims and objectives

At the start of our research, the goal was to create a foam structure for recycled polyethylene terephthalate. In addition to the appropriate injection moulding parameters, the available crystallized blue bottle re-granulate with 4% foaming agent is suitable for forming a closed cell foam structure.

After this our objective was improving the manufactured specimens to achieve the goal: lower density and better mechanical properties. In the comparisons no plain rPET specimens are included, as the current objective is to create better and better foamed samples.

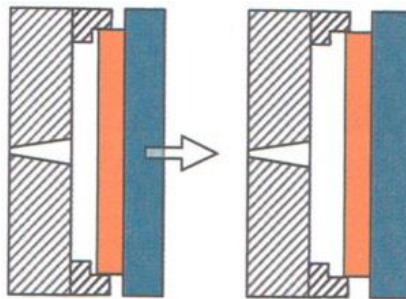


Figure 3. Breathing-mould technique [11]

## 2. Used materials and methods

During the experiments, commercially available blue crystallized PET re-granulate (rPET) was used. The chemical blowing agent was Tracell IM 7200. During injection moulding, 500g of rPET was mixed with 4wt% of chemical blowing agent (CBA). According to the literature research and testing the 4wt% blowing agent produces the best results. The CESA Extend NCA0025531-ZA chain extender was mixed with the substance at 2wt% ratio. Impact modifier used in the testing has been from DuPont at the substance mixture of 10wt%.

During the injection moulding, a dumbbell specimen and a type of thermoplastic polymer material was produced. The Arburg ALLROUNDER 420C Golden Edition injection moulding machine was used to produce the specimens (Table 1). The traditional moulding technology was combined with the breathing tool technology. To achieve the

right tool temperature the samples were tested at 25°C, 35°C and 45°C. The foam structure of the manufactured specimens was examined by YXLON Y.CT Modular Industrial CT. The impact resistance was measured on CEAST 65-45,000 impactors according to MSZ EN ISO 179 standard. The tensile tests were carried out on the INSTRON 5582 universal testing machine according to MSZ EN ISO 527.

*Table 1. Injection moulding parameters*

<i>Description</i>	<i>Unit</i>	<i>Value</i>
Clamp force	kN	150
Nozzle Temperature	°C	260
Injection Pressure	bar	650
Injection Speed	cm <sup>3</sup> /s	30
Holding Pressure 1	bar	150
Holding Pressure 2	bar	50
Holding Time 1	sec	2
Holding Pressure 3	bar	20
Holding Time 2	sec	1
Residual Cooling	sec	0
Intermediate Mould Gap	mm	0.3
Mould Open Delay	sec	20
Mould Temperature	°C	35

## 2.1. Evaluation of results

In our laboratory research, the foam structure, the density and the mechanical properties of the specimens were tested.

## 2.2. Weight, volume and density measurement

In our laboratory research, the extent to which the temperature of the tool temperature is influenced by the density of the undeclared rPET had been tested.

The results showed that the tool temperature, if only to a small degree, had an impact on the density of the specimen. The average 35°C injection moulded specimens were 3.8% higher at 25°C and 3.1% higher in 45°C. Thus, to achieve optimum cell formation, it is advisable to temper the tool to 35°C. (Fig. 4). By means of the foaming and breathing technology, the material fills the tool cavity, but there is some degradation and a decrease in surface quality. The degradations are visible to the naked eye. The reason we used the 35°C tool temperature is as, this proved to be the most effective in terms of cell forming; this is where the most cells have formed and solidified.

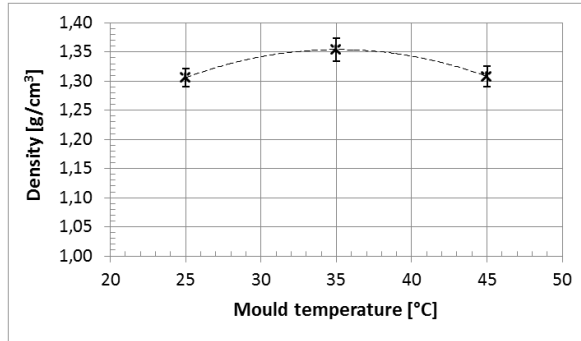


Figure 4. The effect of tool temperature on density in case of rPET

One of the beneficial effects of foaming is the decrease in weight. Because of the established cell structure, the density of the test samples decreases. On average, the density of foamed rPET is 14.82% lower. The density of the rPET expanded with the chain extender was 12.37% less than the non-foamed rPET.

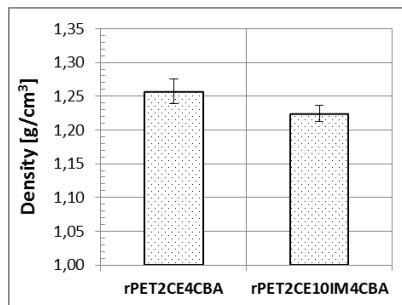


Figure 5. The effect of foamed blend composition on density

I compared the density of the foamed rPET containing the impact modifier and chain-extending agent against only the chain-extended ones. It is apparent from the results that the impact resistance modifier further reduced the mass along with the density (Fig. 5). Concerning cell formation, it can be stated that a better structured cell layout is obtained with increased impact resistance. For density measures the pre-tested specimen has provided data; height, width, length and weight have been measured, from this density can be calculated as follows (1):

$$\rho = \frac{m}{V}, \quad (1)$$

where  $\rho$  [g/cm<sup>3</sup>] is density,  $m$  [g] is weight of the specimen,  $V$  [cm<sup>3</sup>] is the volume of specimen.

### 2.3. Foam structure

After the examination of the foam structure on the specimens with a CT device; Figure 6 shows a 3D image of a 3mm section of rPET specimen with 4wt% chemical blowing agent. The average porosity of the product is 15.05%. The average wall thickness of the

shell wall is 0.526 mm. The cell density of the test samples is 12.67 pcs / mm<sup>3</sup> on average. The average cell diameter is 283µm.

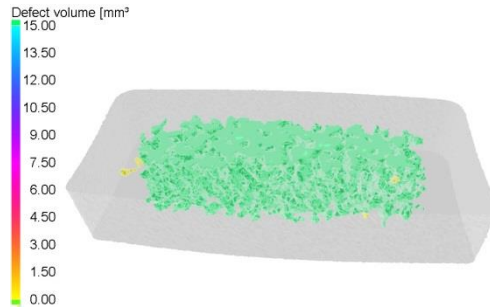


Figure 6. CT images of rPET4CBA

Figure 7 shows the 3D image of a 3mm section of rPET with 4wt% foaming agent and 2wt% chain extender. When calculating the average porosity, a lower value than the test of the no-load test specimens was measured, this value was 12.42%. This is due to the fact that in case of full hollow volume testing, we also received lower values, both cell number and cell density decreased with the chain enhancer. With respect to cell density, 1.116 pcs / mm<sup>3</sup> is the rate of decline. Not only cell numbers but cell diameters are smaller. In the product mixed with the chain extender, the cells have an average diameter of 273 µm. However, the standard deviation of the average cell diameter is relatively high, which is because the core layer has unevenly spread throughout the process.

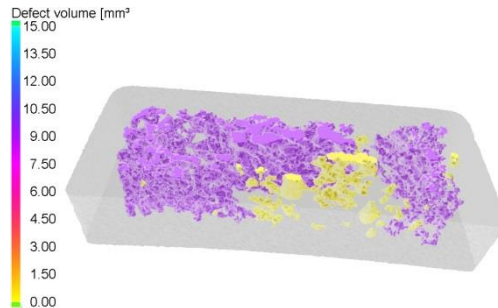


Figure 7. CT images of rPET2CE4CBA

## 2.4. Mechanical testing

We have investigated the effect of the chain extender on the mechanical properties. The results are summarized in Figure 8. As it did not produce the desired results, the mechanical properties with a 10wt% of impact modifier (IM) were compared.

The value of the Young modulus calculated from tensile test results was 47.8% greater than the average of the measured results. After the linearity of tension and deformation ceases, the rPET probes become unstable before the formation of the neck. The deformation would continue in less rigid way, more disorganized structure, but the material that became unstable due to the cells suddenly crashed before the steady flow stage began. Because of the disorderly cell formation, the blend-blown impact exhibits

lower tensile strength. No real elongation was observed in the foamed rPET examination because of the rapid fracture. It can be concluded from the results that although there was a slight increase, but due to the uneven cell formation due to the chain extender, there was a lower elongation. However, the impact resistance increased the elongation value more than twice. Using the impact modifier, a more stable cell structure can be achieved.

In the Charpy impact test, I did not make any notches on the foamed rPET specimens because of the crystal structure and the cellular structure, without the brittle fracture. It can be noticed that the resistance to impact of the 2wt% chain extending agent is greater than that of the foam. The impact modified specimens have three times bigger resistance against dynamical stress as chain extended specimen and seven times greater as pure foam specimen. Thus, it can be stated that the practical use of the impact resistance extender has shown a positive result.

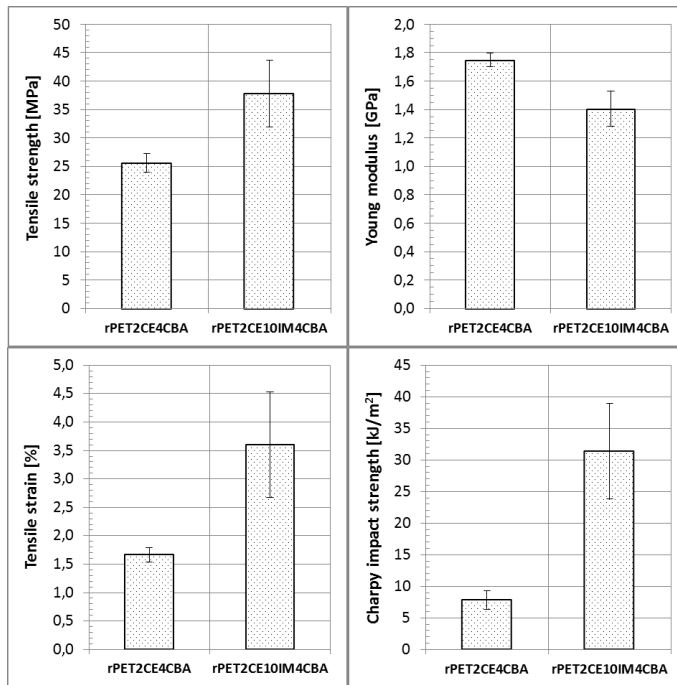


Figure 8. The mechanical properties of foamed rPET

### 3. Conclusion

The aim of the research was to increase the quality of recycled PET with chemical foaming. During our laboratory experiments, we examined the effect of the tool temperature on the injected un-foamed rPET properties. Previous tests have shown that the modification of temperature, changes the mechanical properties of rPET; even if only marginally. By reducing the temperature of the tool, it is more apparent, while the temperature increases resulted tougher plastic. Before processing, the raw material, it

must be dried sufficiently to achieve the appropriate rheological properties. Negative effect that there is some degradation and there is a decline in surface quality, but the increase in density and material utilization as well as a positive effect on weight can be achieved. The use of chain extenders did not produce the desired result. However, the combined application of the impact resistance modifier and the chain extender showed as a positive change in all measured mechanical properties. The new blend showed a seven times better resistance to the initial rPET foam in Charpy's impact test. In the present phase of the research, the test specimens are partly in line with expectations, due to the formation of the cell structure, the result is decreased density. As they are under development in morphological tests positive results were obtained when testing new mixtures. With new chemical blowing agents to test the mixture further mechanical tests are needed. Our further intent is to optimize mechanical properties.

We are confident that after completing the full research, we will define the precise composition and production steps of a substance, which will be a milestone not only for innovative industrial developments but also for environmental protection.

### Acknowledgements

The publishing of this paper was supported by the ÚNKP-16-1 New National Excellence Program of the Ministry of Human Capacities.



EMBERI ERŐFORRÁSOK  
MINISZTERIUMA

### References

- [1] Bach C, Dauchy X, Chagnon M, Serge E: Chemical migration in drinking water stored in polyethylene terephthalate (PET) bottles: a source of controversy, HAL, France 2012
- [2] Coccorullo I, Maio L, Di Montesano S, Incarnato L: Theoretical and experimental study of foaming process with chain extended recycled PET, *Express Polymer Letters*, Vol. 3, No. 2, pp. 84–96, 2009
- [3] Ronkay F, Molnár B, Dogossy G: The effect of mold temperature on chemical foaming of injection molded recycled polyethylene-terephthalate, *Thermochemica Acta*, Vol. 651, pp. 65-72, 2017
- [4] Brandrup J, Immergut EH, Grulke EA: *Polymer Handbook*, Fourth edition, John Wiley & Sons Inc, 1999
- [5] Dobrovcszky K: Upcycling of polymer waste from automotive industry, *Periodica Polytechnica – Mechanical Engineering*, Vol. 55, No. 2, pp. 73-77, 2011
- [6] Belofsky H. *Plastics: Product Design and Process Engineering*, Hanser-Gardner. Munich-Cincinnati, 1995
- [7] Chunxin Z, Florence B, Christian B, Richard M, Christopher L, Hristo A, Albert Y: Highly Porous Polyhedral Silsesquioxane Polymers, *Synthesis and Characterization*, *Journal of the American Chemical Society*, Vol. 120, No. 33, pp. 8380-8391, 1998

- [8] Molnár B: The Effect of Technological Parameters on the Foaming of Injection Molded, Recycled PET, *Acta Technica Jaurinensis*, Vol. 7, No. 1, pp. 1-10, 2014
- [9] Molnár B, Ronkay F: Investigation of Morphology of Recycled PET by Modulated DSC, *Materials Sciences Forum*, Vol. 885, pp. 263-268, 2017
- [10] Molnar B, Ronkay F: Time dependence of morphology and mechanical properties of injection moulded recycled PET, *International Polymer Processing*, Vol. 32, No. 2, pp. 203-208, 2017
- [11] Malnati P.: Innovative Trends in Hybrid Molding Processes, *Plastics Engineering*, Vol. 73, No. 5, pp. 32-37, 2017